Computers and Structures xxx (xxxx) xxx

Contents lists available at ScienceDirect

Computers and Structures

journal homepage: www.elsevier.com/locate/compstruc

Free element collocation method: A new method combining advantages of finite element and mesh free methods

Xiao-Wei Gao, Lan-Fang Gao, Yuan Zhang, Miao Cui, Jun Lv

State Key Laboratory of Structural Analysis for Industrial Equipment, Dalian University of Technology, Dalian 116024, China

ARTICLE INFO

Article history:
Received 27 September 2018
Accepted 3 February 2019
Available online xxxx

Keywords:
Free element collocation method
FECM
Element differential method
Finite element method
Mesh free method
Thermal-mechanical problem

ABSTRACT

In this paper, a new numerical method, named as the Free Element Collocation Method (FECM), is proposed for solving general engineering problems governed by the second order partial differential equations (PDEs). The method belongs to the group of the collocation method, but the spatial partial derivatives of physical quantities are computed based on the isoparametric elements as used in FEM. The key point of the method is that the isoparametric elements used can be freely formed by the nodes around the collocation node. To achieve a narrow bandwidth of the final system of equations, elements with a central node are recommended. For this purpose, a new 21-node quadratic element for 3D problems is constructed for the first time. Attributed to the use of isoparametric elements, FECM can result in more stable results than the traditional collocation method. In addition, the elements can be freely formed by local nodes, FECM has the advantage of mesh-free methods to fit complicated geometries of engineering problems. A number of numerical examples of 2D and 3D thermal and mechanical problems are given to demonstrate the correctness and efficiency of the proposed method.

1. Introduction

As the rapid development of advanced computers, numerical methods become more and more important in design and analysis of practical engineering problems, such as the mechanical, heat transfer, and fluid mechanics problems. In mechanical problems, the dominant numerical method is the finite element method (FEM) [1,2] which is robust and flexible to fit complicated geometries and reflect different material properties. In the heat transfer and fluid mechanics problems, the finite volume method (FVM) [3–6] is the dominant method, attributed to its distinct capability of treating the discontinuous physical phenomena, such as capturing shock waves and implementing upwind scheme. Sometimes, people also like to use the finite difference method (FDM) [7–11] and boundary element method (BEM) [12–16] to solve the heat transfer and fluid mechanics problems. The former is easy to discretize the governing differential equations, and the latter has the advantages of high accuracy and reducing dimensions of the problems. FDM is very easy to use and works well for regular grids. However, when the grids become irregular, the formed coefficient matrix may be singular, and the approximation process can fail. In this case, people need to resort to special algorithms to select nodes to avoid such a singularity issue.

Recent decades, the advanced finite element methods have been developed, such as the extended FEM [17,18] and the strain smoothing FEM [19]. It is also worth mentioning that in order to integrate the robust Computer Aided Design (CAD) tools with the frequently used FEM analysis to increase the efficiency of current engineering workflow, the concept of isogeometric analysis (IGA) was put forward by Hughes et al. [20]. Rapidly, the IGA has been expanded in a number of engineering applications [21–26].

To get rid of the dependency of using elements and meshes, the meshfree method (MFM) [27–35] has obtained an increasingly development for solving the above mentioned problems. A number of the MFMs have been proposed for solving various engineering problems, some of them are weak-form formulations [30–32] having excellent stability, and some of them are strong-form formulations being able to directly discretize the governing equations as done in the point collocation method (PCM) [36–39]. The most distinct advantage of MFMs over FEM and BEM is that no elements or cells are required to solve an engineering problem governed by PDEs [27–29], which is extremely convenient to solve problems with complicated geometries or moving boundaries [29]. There are two types of MFMs [28], strong-form and weak-form approaches. The strong-form MFMs are the simplest collocation approach, which is very straightforward to use in solving PDEs. However, there is the stability problem for some of them [28], that is, the solution may be dependent on the number and distribution

E-mail address: xwgao@dlut.edu.cn (X.-W. Gao)

https://doi.org/10.1016/j.compstruc.2019.02.002
0045-7949/

of the computational nodes. The weak-form MFMs have good stability due to reducing the order of the spatial derivatives through an integration scheme, but they need the integration over back ground meshes or cells [40,41] which may injure the reputation of the MFM that no elements are required. In some methods, the integration can be avoided by using some particular treatments [42].

In MFMs, a cluster of nodes around the computational node are locally selected for computing the global shape functions which are used to approximate physical variables. Since most global shape functions constructed in MFMs do not satisfy the characteristic of the Delta symbol, the intrinsic difficulty exists in MFMs to impose boundary conditions, especially the natural boundary conditions. A few effective approaches have been proposed for imposing the boundary conditions in literature [28].

A different MFM has been proposed by Yagawa and co-workers [43,44], which is called the free mesh method (FMM). In FMM, a set of local meshes is generated for triangular elements formed from the collocation node (central node) and the so called satellite nodes. Similar to the standard PCM, FMM uses node by node processing to set up the system of equations and has the advantage of easily generating local meshes. Since the triangular elements are employed to establish the weak-form solution system, FMM has the weakness of using high-order elements. To overcome this weakness, the enriched free mesh method has been proposed [45,46] for improving the computational accuracy of FMM.

Recently, a new type of element-based method, element differential method (EDM), is proposed by Gao et al. [47,48] for solving general boundary value problems governed by the second order PDEs based on the use of Lagrange isoparametric elements as used in the standard FEM as well as in the newly proposed strong-form methods FBM [49,50] and SFEM [51–58]. In the element-based methods, such as FEM and EDM, shape functions are created based on regular elements (square, cube, etc.) represented in the natural (intrinsic) coordinate system. A mapping procedure links the regular element to the physical irregular element via a Jacobian matrix [1,39,49,52–58]. The advantage of using the element-based methods is that a stable solution can be easily obtained, provided the element is not distorted heavily [1,2]. The another benefit from the use of the finite elements is that the local sub-domains for approximation of field variables can be easily formed from the predefined or automatically generated elements as used in the numerical implementation of the local integral equation formulation [59–61]. The distinct feature of EDM presented in [47,48] is that a set of analytical expressions for the first and second partial derivatives of general shape functions with respect to the global coordinates are derived, which make EDM a stable and fast collocation method. The fixed isoparametric elements are used in EDM and the system of equations can be easily formed by directly substituting the derived second and first order global spatial derivatives of shape functions into the governing equations and boundary conditions, respectively. All elements connected with the collocation node are computed in EDM and the final system of equations is formed based on the traction/flux equilibrium conditions by adding each element's contribution together. EDM is a kind of the strong-form element collocation method, having the advantage of easy application in complicated PDEs. The drawback of EDM is that the resulted system has a wide bandwidth when using high order elements.

In this paper, a new method, called the Free Element Collocation Method (FECM) [62,63], is proposed by absorbing the advantages of EDM and FMM. From EDM, the analytical expressions for global spatial derivatives based on isoparametric elements are adopted in FECM to generate the system of equations from the governing equations by using a direct collocation scheme. And as in FMM, the local isoparametric elements used in FECM can be freely formed by the collocation node and around nodes. What the differences of FECM from EDM are that (1) the freely formed local elements are used in FECM rather than using fixed elements, which makes the element generation easier; and (2) only one element including the collocation node is required in FECM, which can make the bandwidth of the system of equations much smaller than EDM, even smaller than the standard FEM. Another difference between FECM and EDM is that the governing equation of the problem is collocated at all internal nodes of the problem in FECM, but it is only collocated at elements' internal nodes in EDM. The difference of FECM from FMM is that only one local isoparametric element is needed for each collocation node in FECM, but in FMM a local mesh consisting of a number of triangular elements around the collocation node is used. This feature not only can make FECM have an extremely narrow bandwidth of the system, but also can make FECM be able to use high order elements naturally.

In the paper, although the heat conduction and solid mechanics problems are considered, the presented formulations and methodology can also be used to solve other engineering problems governed by the first and second order PDEs.

The paper is arranged as follows: firstly the governing equations and imposed boundary conditions for heat conduction and solid mechanics are presented in Section 2; and then the typical isoparametric elements used in the paper are given in Section 3 where a new element, the 21-node hexahedron element, is also constructed for the first time; and followed by Section 4 is a review of the analytical expressions used to compute the global spatial derivatives; in Section 5 a detailed description of the proposed new method, FECM, is carried out; in Section 6 a few 2D and 3D numerical examples on thermal and mechanical problems are given to demonstrate the correctness and efficiency of the proposed method; and finally the concluding discussions are drawn in Section 7.

2. Governing equations for thermal and mechanical problems

Most engineering problems are governed by a set of simultaneous second-order PDEs, with a proper set of boundary conditions for physical variables (temperature, displacement) and physical variable gradient related quantities (flux, traction). For example, in the heat conduction problem, the governing equation is given by the Fourier law [3,47], and in the elasticity problem, the governing equations are the Navier-Cauchy Equations of Equilibrium [1,2]. Both are the second order PDEs.

2.1. Governing equations and boundary conditions for heat conduction problems

The governing equation for general steady state heat conduction problems can be expressed as [47]:

$$\frac{\partial}{\partial x_i}\left(\lambda_{ij}(\boldsymbol{x})\frac{\partial T(\boldsymbol{x})}{\partial x_j}\right)+Q(\boldsymbol{x})=0,\quad \boldsymbol{x}\in\Omega \tag{1}$$

where $\boldsymbol{x}$ represents a point located in the computational domain Ω, x_i is the i-th component of the spatial coordinates defined at the point $\boldsymbol{x}$, λ_{ij} the thermal conductivity with the symmetry of $\lambda_{ij}=\lambda_{ji}$, T the temperature, Q the heat-generation rate. The repeated subscripts i and j represent the summation through its range which is 2 for 2D and 3 for 3D problems.

The boundary conditions of the problem can be described as follows:

$$T(\boldsymbol{x})=\bar{T}\quad \boldsymbol{x}\in\Gamma_1 \tag{2}$$

$$q(\boldsymbol{x})=-\lambda_{ij}(\boldsymbol{x})\frac{\partial T(\boldsymbol{x})}{\partial x_j}n_i(\boldsymbol{x})=\bar{q}\quad \boldsymbol{x}\in\Gamma_2 \tag{3a}$$

Please cite this article as: X.-W. Gao, L. F. Gao, Y. Zhang et al., Free element collocation method: A new method combining advantages of finite element and mesh free methods, Computers and Structures, https://doi.org/10.1016/j.compstruc.2019.02.002

$$q(\boldsymbol{x}) = -\lambda_{ij}(\boldsymbol{x})\frac{\partial T(\boldsymbol{x})}{\partial x_j}n_i(\boldsymbol{x}) = h(T(\boldsymbol{x}) - T_\infty) \quad \boldsymbol{x} \in \Gamma_3 \tag{3b}$$

in which, $\Gamma_1 \cup \Gamma_2 \cup \Gamma_3 = \Gamma$, $\Gamma = \partial\Omega$, n_i is the i-th component of the outward normal to the boundary Γ, h is the heat transfer coefficient; $\bar{T}$,$\bar{q}$ and T_∞ arn the prescribed temperature, heat flux and environmental temperature on the boundary, respectively.

2.2. Governing equations and boundary conditions for thermal-mechanics problems

The governing equations for thermal-mechanics problems is described by the following equilibrium equation [1,48]:

$$\frac{\partial}{\partial x_j}\left(D_{ijkl}(\boldsymbol{x})\frac{\partial u_k(\boldsymbol{x})}{\partial x_l}\right) - \frac{\partial\left(\tilde{k}(\boldsymbol{x})T(\boldsymbol{x})\right)}{\partial x_i} + b_i(\boldsymbol{x}) = 0, \qquad \boldsymbol{x} \in \Omega \tag{4}$$

where u_k is the displacement, b_i the body force, D_{ijkl} is the stress-strain constitutive tensor with the symmetry of $D_{ijkl} = D_{jikl} = D_{ijlk} = D_{klij}$. For inhomogeneous problems, D_{ijkl} is the function of coordinates [15]; for non-linear problems, e.g. the elastoplasticity problems, D_{ijkl} is the function of stresses or strains [1,64]; and for linear elasticity problems, D_{ijkl} is a constant tensor and can be expressed as [42]

$$D_{ijkl} = \lambda\delta_{ij}\delta_{kl} + \mu\left(\delta_{ik}\delta_{jl} + \delta_{il}\delta_{jk}\right) \tag{5}$$

where

$$\lambda = \frac{2\mu\nu}{(1-2\nu)} \tag{6a}$$

$$\tilde{k} = \frac{2\mu(1+\nu)}{1-2\nu}k \tag{6b}$$

in which, μ is the shear modulus, ν the Poisson ration, k the coefficient of thermal expansion.

The boundary conditions for thermal-mechanics problems can be described by the following expressions:

$$u_i(\boldsymbol{x}) = \bar{u}_i(\boldsymbol{x}), \qquad \boldsymbol{x} \in \Gamma_u \tag{7}$$

$$t_i(\boldsymbol{x}) = D_{ijkl}(\boldsymbol{x})n_j(\boldsymbol{x})\frac{\partial u_k(\boldsymbol{x})}{\partial x_l} - \tilde{k}(\boldsymbol{x})T(\boldsymbol{x})n_i(\boldsymbol{x}) = \bar{t}_i, \qquad \boldsymbol{x} \in \Gamma_t \tag{8}$$

where t_i is the i-th traction component, Γ_u and Γ_t are the boundaries specified by displacement $\bar{u}_i$ and traction $\bar{t}_i$, respectively, with $\Gamma_u \cup \Gamma_t = \Gamma$. The relationship expressed by Eq. (8) is also called the traction equilibrium equation.

In mathematics, the boundary conditions shown in Eqs. (2) and (7) are related to the physical variables them-self and are called the Dirichlet boundary conditions. The boundary conditions shown in Eqs. (3) and (8) are related to the gradients of the physical variables and are called the Neumann boundary conditions. From Eqs. (1) and (4), it can be seen that the governing equations for thermal and mechanics problems are the second order PDEs of the physical variables, temperature and displacement. And the boundary conditions shown in Eqs. (3) and (8) indicate that the flux and traction are related to the first order partial derivatives of the physical variables. Therefore, the key task of solving such problems is to set up a scheme to compute the first and second order spatial partial derivatives of the physical variables. The successful experience of applying FEM to solve various engineering problems tell us that the use of regularly shaped isoparametric elements to compute the spatial derivatives can achieve very stable results. In view of this, the authors in [47,48] proposed a method to derive the analytical expressions of computing the first and second order spatial partial derivatives based on the Lagrange isoparametric elements. In the following section, this method will be reviewed, and a new robust method, called the free element collocation method, will be proposed to solve general engineering problems based on the Lagrange and non-Lagrange isoparametric elements.

3. Isoparametric elements used in free element collocation mehtod

The isoparametric elements used in FEM [1,2] have excellent characteristics in geometry representation and physical variable interpolation. From Eqs. (1) and (4), it can be seen that the second order spatial partial derivatives are included in the governing equations. Therefore, at least the quadratic elements should be used in FECM to ensure the second order spatial derivatives non-zero. Although all high order isoparametric elements used in FEM can be used in FECM, only a few 2D and 3D quadratic elements are presented in the paper.

3.1. The 9-node 2D Lagrange isoparametric element

The frequently used two-dimensional isoparametric elements are the 8-node serendipity and 9-node Lagrange elements. The former can be found in most FEM books (e.g. [1,2]) and the latter is shown in Fig. 1 which will be used in this study. More high order elements can be found in [47–55]. The shape functions for these elements can be found in most FEM [1,2] or BEM book [64].

3.2. The 27-node 3D isoparametric element

The typical 3D quadratic isoparametric elements are the 20-node serendipity and 27-node Lagrange hexahedron elements. The former can be in references [1,2] and the latter is shown in Fig. 2. The shape functions for these two elements can be found in [1,48,64], respectively.

3.3. The 21-node 3D quadratic isoparametric element

In the paper, the governing equations, such as Eqs. (1) and (4) in the thermal and solid mechanics problems, are collocated node by node. If elements without internal nodes, such as the 8-node 2D rectangular element and the 20-node 3D hexahedron element [1,2], are used to compute the spatial derivatives, the collocation node must be placed at one of the corner or edge nodes. This may result in poor values of the derivatives. On the other hand, if the collocation node is located at an internal node of an element,

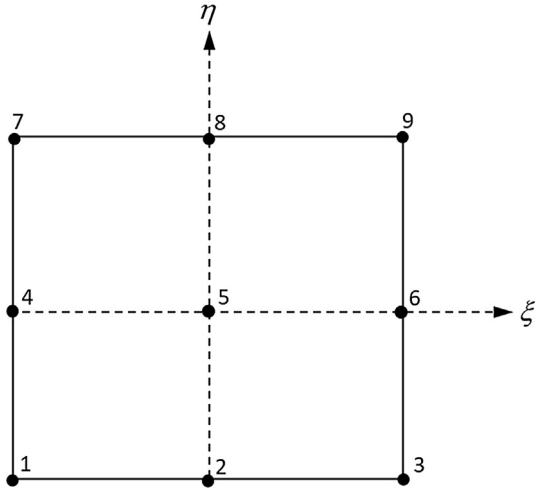

Fig. 1. The 9-node 2D Lagrange element.

Please cite this article as: X.-W. Gao, L. F. Gao, Y. Zhang et al., Free element collocation method: A new method combining advantages of finite element and mesh free methods, Computers and Structures, https://doi.org/10.1016/j.compstruc.2019.02.002

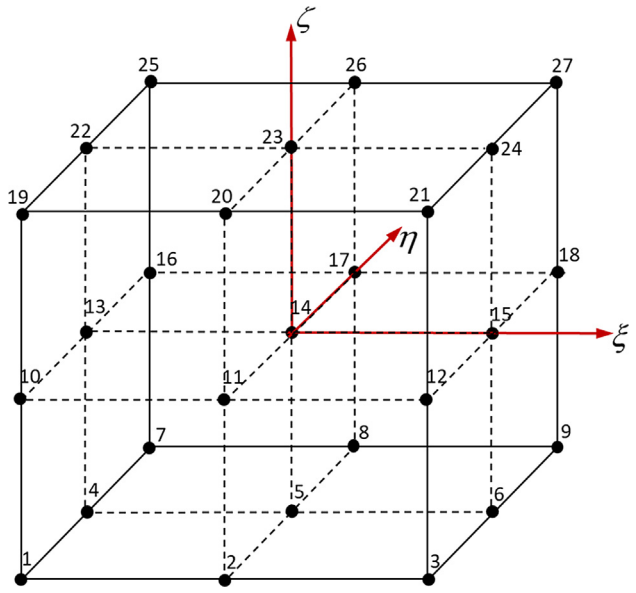

Fig. 2. The 27-node 3D Lagrange element.

such as the central node in Figs. 1 and 2, the computational accuracy of the spatial derivatives is higher. However, the 27-node Lagrange hexahedron element shown in Fig. 2 has too many nodes. Therefore, a new quadratic element with less nodes, the 21-node element, is constructed in the paper, which has one internal node numbered as node 21 and is shown in Fig. 3. The construction method of the shape functions for the 21-node element is similar to that of other serendipity elements [1], which has been listed in the Appendix of this paper.

4. Element differential formulations

Over each above presented isoparametric element, the variation of any quantities can be expressed in terms of their nodal values of the element [47,48]. For example, the spatial coordinates, temperature and displacement can be expressed as

$$x_i = N_\alpha x_i^\alpha \tag{9a}$$

$$T = N_\alpha T_\alpha \tag{9b}$$

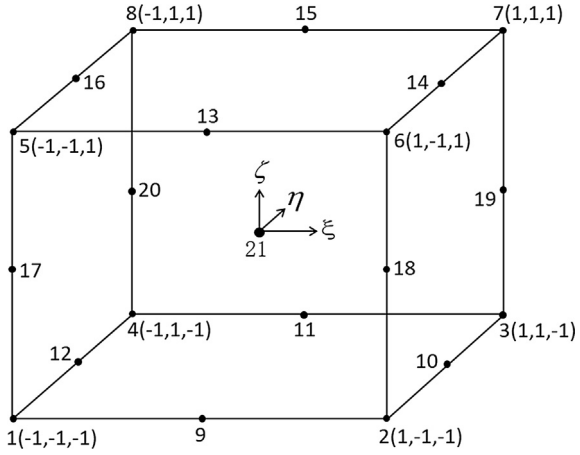

Fig. 3. The 21-node 3D hexahedron element.

$$u_i = N_\alpha u_i^\alpha \tag{9c}$$

where x_i^α, T^α and u_i^α are the values of coordinates, temperature and displacements at node α, and the repeated index α represents the summation over all elemental nodes.

Thus, the first and second order global spatial partial derivatives can be shifted to the shape functions. For example, the derivatives of temperature can be expressed as

$$\frac{\partial T}{\partial x_i} = \frac{\partial N_\alpha}{\partial x_i} T^\alpha \tag{10}$$

$$\frac{\partial^2 T}{\partial x_i \partial x_j} = \frac{\partial^2 N_\alpha}{\partial x_i \partial x_j} T^\alpha \tag{11}$$

Based on Eqs. (10) and (11), and noticing that the shape functions N_α are the explicit functions of the intrinsic coordinates ξ_k, it can be derived [47,48] that

$$\frac{\partial N_\alpha}{\partial x_i} = [J]^{-1}_{ik} \frac{\partial N_\alpha}{\partial \xi_k} \tag{12}$$

$$\frac{\partial^2 N_\alpha}{\partial x_i \partial x_j} = \left[[J]^{-1}_{ik} \frac{\partial^2 N_\alpha}{\partial \xi_k \partial \xi_l} + \frac{\partial [J]^{-1}_{ik}}{\partial \xi_l} \frac{\partial N_\alpha}{\partial \xi_k} \right] [J]^{-1}_{jl} \tag{13}$$

where $[J] = [\partial \boldsymbol{x} / \partial \boldsymbol{\xi}]$ is the Jacobian matrix mapping from the global coordinate system x_i to the intrinsic coordinate system ξ_k, with $(x_1, x_2) = (x, y)$ and $(\xi_1, \xi_2) = (\xi, \eta)$ for 2D problems, and $(x_1, x_2, x_3) = (x, y, z)$ and $(\xi_1, \xi_2, \xi_3) = (\xi, \eta, \varsigma)$for 3D problems. The Jacobian matrix $[J]$ can be easily computed using the following expression:

$$[J]_{ik} = \left[\frac{\partial \boldsymbol{x}}{\partial \boldsymbol{\xi}} \right]_{ik} = \frac{\partial x_i}{\partial \xi_k} = \frac{\partial N_\alpha}{\partial \xi_k} x_i^\alpha \tag{14}$$

And the inverse matrix of $[J]$ can be written as the following form:

$$[J]^{-1} = \left[\frac{\partial \boldsymbol{\xi}}{\partial \boldsymbol{x}} \right] = \frac{1}{|J|} [A] \tag{15}$$

where

$$[A] = \begin{bmatrix} y_\eta & -y_\xi \\ -x_\eta & x_\xi \end{bmatrix} \tag{16}$$

$$|J| = x_\xi y_\eta - x_\eta y_\xi \tag{17}$$

for 2D problems, and

$$[A] = \begin{bmatrix} y_\eta z_\varsigma - y_\varsigma z_\eta & y_\varsigma z_\xi - y_\xi z_\varsigma & y_\xi z_\eta - y_\eta z_\xi \\ x_\varsigma z_\eta - x_\eta z_\varsigma & x_\xi z_\varsigma - x_\varsigma z_\xi & x_\eta z_\xi - x_\xi z_\eta \\ x_\eta y_\varsigma - x_\varsigma y_\eta & x_\varsigma y_\xi - x_\xi y_\varsigma & x_\xi y_\eta - x_\eta y_\xi \end{bmatrix} \tag{18}$$

$$|J| = x_\xi y_\eta z_\varsigma - x_\eta y_\xi z_\varsigma - x_\xi y_\varsigma z_\eta + x_\varsigma y_\xi z_\eta + x_\eta y_\varsigma z_\xi - x_\varsigma y_\eta z_\xi \tag{19}$$

for 3D problems.

In above equations, $z_\eta = \partial z / \partial \eta = (\partial N_\alpha / \partial \eta) z^\alpha$, and the same meaning can be applied to other terms.

Thus, differentiating Eq. (15) leads to

$$\frac{\partial [J]^{-1}}{\partial \xi_l} = \frac{1}{|J|} \frac{\partial [A]}{\partial \xi_l} - \frac{1}{|J|^2} \frac{\partial |J|}{\partial \xi_l} [A] \tag{20}$$

The detailed analytical expressions about $\frac{\partial [A]}{\partial \xi_l}$ and $\frac{\partial |J|}{\partial \xi_l}$ appearing in the above equation can be found in [47,48]. The terms $\frac{\partial N_\alpha}{\partial \xi_k}$ and $\frac{\partial^2 N_\alpha}{\partial \xi_k \partial \xi_l}$ in Eqs. (12) and (13) can be easily obtained by directly differentiating the shape functions of the used element.

Using the above element differential formulation, the first and second order partial derivatives of shape functions with respect

Please cite this article as: X.-W. Gao, L. F. Gao, Y. Zhang et al., Free element collocation method: A new method combining advantages of finite element and mesh free methods, Computers and Structures, https://doi.org/10.1016/j.compstruc.2019.02.002

to the global coordinates can be computed accurately. It has been shown by numerical examples [47,48] that satisfactory results can be obtained even for a highly distorted element.

Based on the above presented formulations, a system of equations can be formed by substituting them into the governing equations and boundary conditions, which will be described in the following section in depth.

5. Free element collocation method to form the system of equations

When solving an engineering problem governed by the partial differential equations as shown in Eqs. (1) and (4) using FECM, the computational domain Ω is discretized into a series of distributed nodes. The system of equations is established node by node. For each node which is called the collocation node (CN) for convenience, a local isoparametric element which is called the collocation element is formed by the CN and surround nodes. The nodes to form the collocation element can be freely selected. However, to achieve a high computational accuracy, the selected nodes are able to form the element with the shape as regular as possible to satisfy the requirement of the elements shown in Figs. 1–3. According to the geometric position of the CN, different positions may be located by the CN over the formed element. Three types of the positions of CN may be classified: internal nodes, smooth boundary nodes, and corner nodes, which are illustrated in Fig. 4 for the 2D problem using the 9-node Lagrange element as the collocation element.

For internal nodes of the problem, the CN should be the central node of the formed collocation element. For smooth nodes, the CN should be the central node of the side (2D) or the surface (3D) over which the CN is located. And for a corner node, the CN has to be one of the element corner nodes.

In this collocation scheme, it can be seen that each node uses its own collocation element. Eventually, all used elements form an overlapped element pattern.

Because nodes-non-equally-spaced elements have excellent behavior in simulating irregularly distributed points, the nodes-non-equally-spaced Lagrange elements are used in the paper by defining the nodal parametric coordinates based on the distances between adjacent elemental nodes.

After the element including the CN is formed in the way described above, the system of equations can be generated according to CN's position located inside or on the boundary of the problem, which is described in the following.

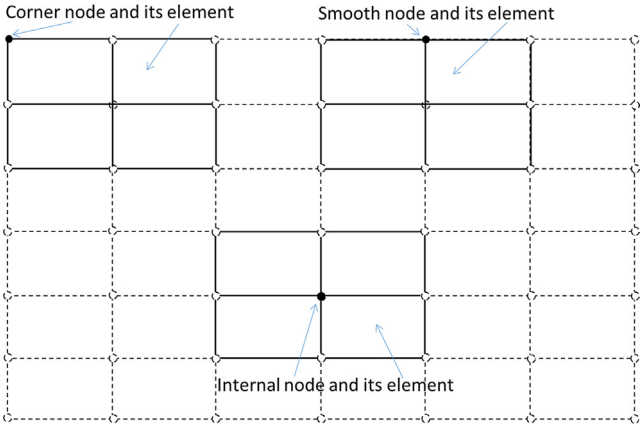

Fig. 4. Schematic show of three kind of 9-node collocation elements for different collocation nodes in the 2D problems.

5.1. Collocating equations for internal nodes

As mentioned above, the system of equations is formed node by node in FECM. For nodes located inside the domain of the problem, the governing Eqs. (1) and (4) are collocated at each node by using a locally formed collocation element as shown in Fig. 4. To do this, Eqs. (1) and (4) can be rewritten as:

$$\lambda_{ij}(\boldsymbol{x})\frac{\partial^2 T(\boldsymbol{x})}{\partial x_i \partial x_j}+\frac{\partial \lambda_{ij}(\boldsymbol{x})}{\partial x_i}\frac{\partial T(\boldsymbol{x})}{\partial x_j}+Q(\boldsymbol{x})=0 \tag{21}$$

$$D_{ijkl}(\boldsymbol{x})\frac{\partial^2 u_k(\boldsymbol{x})}{\partial x_l \partial x_j}+\frac{\partial D_{ijkl}(\boldsymbol{x})}{\partial x_j}\frac{\partial u_k(\boldsymbol{x})}{\partial x_l}-\frac{\partial\left(\tilde{k}(\boldsymbol{x})T(\boldsymbol{x})\right)}{\partial x_i}+b_i(\boldsymbol{x})=0 \tag{22}$$

Thus, on substituting Eqs. (10) and (11) into the above equations, it follows that

$$\left[\lambda_{ij}(\xi)\frac{\partial^2 N_\alpha(\xi^c)}{\partial x_i \partial x_j}+\frac{\partial \lambda_{ij}(\xi^c)}{\partial x_i}\frac{\partial N_\alpha(\xi^c)}{\partial x_j}\right]T^\alpha+Q(\xi^c)=0 \tag{23}$$

for heat conduction problems, and

$$\left[D_{ijkl}(\xi^c)\frac{\partial^2 N_\alpha(\xi^c)}{\partial x_l \partial x_j}+\frac{\partial D_{ijkl}(\xi^c)}{\partial x_j}\frac{\partial N_\alpha(\xi^c)}{\partial x_l}\right]u_k^\alpha-\frac{\partial N_\alpha(\xi^c)}{\partial x_i}\tilde{k}^\alpha T^\alpha+b_i(\xi^c)=0 \tag{24}$$

for thermal-mechanics problems.

In the above equations, ξ^c is the intrinsic coordinate at the central node of the locally formed collocation element.

The term $\partial\lambda_{ij}/\partial x_i$ and $\partial D_{ijkl}/\partial x_j$ in Eqs. (23) and (24) can be calculated through the direct differentiation manner, if the analytical expression of the λ_{ij} and D_{ijkl} are given. Otherwise, the following expressions can be used to compute their values numerically.

$$\frac{\partial \lambda_{ij}(\xi^c)}{\partial x_i}=\frac{\partial N_\beta(\xi^c)}{\partial x_i}\lambda_{ij}^\beta \tag{25a}$$

$$\frac{\partial D_{ijkl}(\xi^c)}{\partial x_j}=\frac{\partial N_\beta(\xi^c)}{\partial x_j}D_{ijkl}^\beta \tag{25b}$$

where λ_{ij}^β and D_{ijkl}^β are the values of λ_{ij} and D_{ijkl} at the β-*th* element node.

In the evaluation of the spatial derivatives numerically based on isoparametric elements, the computational accuracy is higher for internal nodes than that for boundary nodes of the elements. Therefore, elements with a central node such as the elements shown in Figs. 1–3 is recommend for the case of the internal collocation node.

5.2. Collocating equations for boundary nodes

For a node located on the boundary of the problem, the Neumann boundary conditions, that is, the relationships between flux/traction and gradients of the temperature/displacement as shown in Eqs. (3) and (8), are used to generate the system of equations. For a boundary node, it also must be a boundary node of the collocation element (see Fig. 4). For such a node, the accuracy of the computed values of the spatial derivatives is lower than the node located inside the element. Fortunately, only the first order spatial derivatives are needed for the boundary nodes (see Eqs. (3) and (8)).

Thus, substituting Eqs. (10) and (11) into Eqs. (3) and (8) yields:

$$q(\xi^b)=-\lambda_{ij}(\xi^b)\frac{\partial N_\alpha(\xi^b)}{\partial x_j}n_i(\xi^b)T^\alpha \tag{26}$$

for heat conduction problems, and

Please cite this article as: X.-W. Gao, L. F. Gao, Y. Zhang et al., Free element collocation method: A new method combining advantages of finite element and mesh free methods, Computers and Structures, https://doi.org/10.1016/j.compstruc.2019.02.002

$$t_i(\xi^b) = D_{ijkl}(\xi^b)n_j(\xi^b)\frac{\partial N_\alpha(\xi^b)}{\partial x_l}u_k^\alpha - \tilde{k}(\xi^b)T(\xi^b)n_i(\xi^b) \tag{27}$$

for thermal-mechanics problems.

In the above equations, ξ^b is the intrinsic coordinate of the collocation element node at which the collocation node is located, the n_i is the outward normal to the boundary of the element.

It is noted that when the collocation node is located on the boundary of the problem, the node has to be one of the boundary nodes of the collocation element. Therefore, the elements without internal nodes such as those used in the standard FEM [1,2] can also be used for boundary collocation nodes, apart from the elements with internal nodes.

Another important issue needing to be addressed when collocating the boundary nodes using the Neumann boundary conditions is that the outward unit normal vector $\boldsymbol{n}$ appearing in the collocation equations (see Eqs. (26) and (27)) is discontinuous at corner or edge nodes [52,59–61]. Therefore, although one locally formed independent collocation element is used for each boundary node in FECM, different surfaces characterized with different outward normal vectors may exist at the same corner or edge node located on the same collocation element. In this case, a number of independent surface equations can be setup using Eq. (26) or (27) for different surfaces. To obtain a set of equations for each corner or edge node, the method described in [47,48] is employed to treat such a case, that is, adding all these surface equations together to form one set of independent equations for the corner or edge node. The details about this method can be found in [47,48]. As for the outward normal vector $\boldsymbol{n}$, the commonly used techniques in BEM [12,64] is employed in this study to determine the outward normal vector to a curved line or a curved surface.

Based on Eqs. (23) and (24) as well as Eqs. (26) and (27), the system of equations can be formed by applying proper boundary conditions.

5.3. Forming the system of equations

For each internal node, Eq. (23) or (24) can generate an equation involving nodal values of temperature/displacement over all nodes of the used collocation element. And for each boundary node, Eq. (26) or (27) can generate an equation involving nodal temperatures/displacements as well as boundary fluxes/tractions. To build the final system of equations, a global nodal vector $\boldsymbol{U}$ consisting of temperatures/displacements at all nodes numbered in the global nodal sequence is defined. Each of the elemental node α appearing in Eqs. (23) and (24) as well as Eqs. (26) and (27) corresponds to a position in the global nodal vector $\boldsymbol{U}$. For every boundary node, either the temperature/displacement or the flux/traction should be specified as the Dirichlet or Neumann boundary conditions. These boundary conditions can be directly imposed on the formed system of equations, since the shape functions of the used free elements satisfy the Delta symbol characteristic. Thus, after applying the boundary conditions to each generated equation, the following system of algebraic equations can be formed:

$$\boldsymbol{KU} = \boldsymbol{P} \tag{28}$$

where $\boldsymbol{P}$ is a known vector formed by the given heat fluxes or tractions of the nodes at which the flux/traction boundary conditions are specified, $\boldsymbol{K}$ is formed by the coefficients of Eqs. (23)/(24) and (26)/(27) for conduction/mechanics problems. It is noted that for the nodes at which the temperatures/displacements are specified, the columns of the matrix $\boldsymbol{K}$ corresponding to these nodes are taken as 0 except for the diagonal ones which are taken as 1. In this case, the given temperatures/displacements are multiplied with their corresponding coefficients in Eqs. (23)/(24) and (26)/(27) and have been included in the right-hand side term $\boldsymbol{P}$ of Eq. (28). For the nodes at which the temperatures/displacements are specified, the corresponding positions in the vector $\boldsymbol{P}$ should be the values of the specified temperatures/displacements. This type of treatment is similar to that in FEM [1,2].

Assume that the total number of nodes is N, then the size of the coefficient matrix $\boldsymbol{K}$ in Eq. (28) is $N \times N$ for 2D and 3D heat conduction problems. And, for solid mechanics problems, $\boldsymbol{K}$ is a $2N \times 2N$ matrix for 2D problems or a $3N \times 3N$ matrix for 3D problems.

It is noted that in each generated equation from Eqs. (23)/(24) and (26)/(27), only coefficients corresponding to the nodes of the elements associated with the collocation node are not zero. Therefore, the matrix $\boldsymbol{K}$ in Eq. (28) is highly sparse.

Since the isoparametric elements as used in the standard FEM are used in the paper, the condition number of the system matrix is similar to that in FEM, which depend on the distribution of the elemental nodes. The more regular the distribution of nodes are, the better the number of the system matrix is. One of the advantages of the proposed FECM is that the element for each collocation node can be formed locally by freely selecting surround nodes and this gives us the opportunity to form a regular element for each node.

5.4. Evaluation of heat flux vectors and stresses

After all temperatures/displacements at boundary and internal nodes are solved from Eq. (28), the heat flux vector and stresses can be easily calculated using the following expressions:

$$q_i(\xi^n) = -\lambda_{ij}(\xi^n)\frac{\partial N_\alpha(\xi^n)}{\partial x_j}T^\alpha \tag{29}$$

$$\sigma_{ij}(\xi^n) = D_{ijkl}(\xi^n)\frac{\partial N_\alpha(\xi^n)}{\partial x_l}u_k^\alpha - \tilde{k}(\xi^n)T(\xi^n) \tag{30}$$

where ξ^n is the intrinsic coordinate of the elemental node n to be calculated.

5.5. Implement procedure of the proposed methodology

To make the proposed methodology clearer, a flowchart of the implement procedure has been drawn as shown in Fig. 5, following which is a detailed description.

The following is a one by one description of the flowchart shown in Fig. 5, in which the numbers correspond to the superscript numbers shown in Fig. 5 for each item.

(1) The computational model used in FECM is similar to that of EDM in [48]. The main difference is that only one element is formed for one node. In current study, the model is firstly set up by ANSYS, and then it is transformed into the FECM model by a self-developed code. All the elements are pre-generated and stored in the hard disk and retrieved when using them.
(2) The system of equations are formed by collocating governing equations at internal nodes and the boundary conditions at boundary nodes. The computation is performed through a node loop procedure. When the computation is finished for a node, the system of equations for this node is completely set up. Therefore, the method is very suitable for parallel computing.
(3) When the collocation node is an internal node, the governing Eq. (23) or (24) is used to directly form the equations of the global system. In this computation, the source term $Q(\boldsymbol{x})$ or the body force term $b_i(\boldsymbol{x})$ in them are directly evaluated using the coordinates at the current collocation node.

Please cite this article as: X.-W. Gao, L. F. Gao, Y. Zhang et al., Free element collocation method: A new method combining advantages of finite element and mesh free methods, Computers and Structures, https://doi.org/10.1016/j.compstruc.2019.02.002

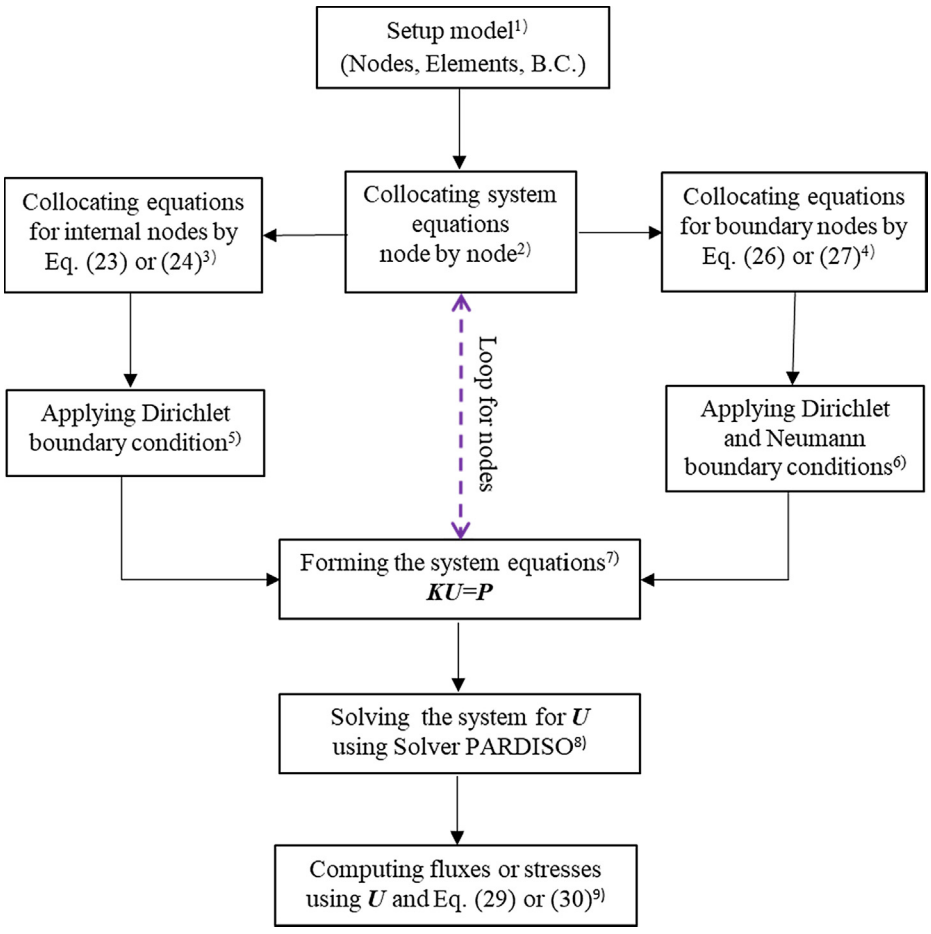

Fig. 5. Flowchart for the implement of FECM.

(4) When the collocation node is an outer boundary node, the Neumann boundary condition (26) or (27) is used to generate the equations of the global system.
(5) When collocating the internal nodes, if some of the related elemental nodes are on the boundary and the Dirichlet boundary conditions are specified at these nodes, the specified values of temperature or displacement are multiplied with their corresponding coefficients and are incorporated into the vector $\boldsymbol{P}$ of the system equation $\boldsymbol{KU = P}$.
(6) When collocating the boundary nodes, the Neumann condition is used to generate the equations of the global system. However, if the Dirichlet condition is specified for the current collocation node, this boundary node is skipped for collocation. In this case, the specified values will be particularly treated in a manner as described in the next item. On the other hand, if the collocation node is not specified with the Dirichlet boundary condition, but some of the related elemental nodes are, the specified temperature or displacement should be incorporated in the vector $\boldsymbol{P}$.
(7) When the nodal loop is finished for all nodes, the final system of equations, $\boldsymbol{KU = P}$, is generated. For nodes over which the Dirichlet boundary conditions are specified, the diagonal terms of the system matrix $\boldsymbol{K}$ corresponding to these nodes should be put as *1* and all other elements in the corresponding columns should be put as *0*. Besides, for these nodes, the corresponding positions in vector $\boldsymbol{P}$ should be the specified values of temperature or displacement.
(8) Although the system of equations shown in Eq. (28) is not symmetric, since only one element is used for each node, the system matrix $\boldsymbol{K}$ is extremely sparse. Thus, the equation solver named PARDISO built in the MKL library of the Intel Fortran compiler 11.0 can be used to effectively solve this type of system.
(9) Once the temperatures or displacements at all nodes are solved from the system of $\boldsymbol{KU = P}$, the heat fluxes or stresses at any nodes can be evaluated using Eqs. (29) or (30). Thus, all thermal or mechanical quantities can be obtained.

6. Numerical examples

To validate the correctness and application potential of the proposed method, a Fortran code has been developed and compiled with the Intel Fortran compiler (version 11.0). And four numerical

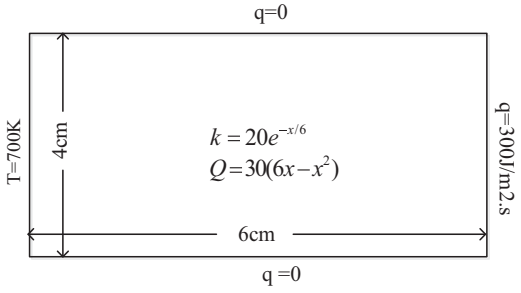

Fig. 6. Dimension and boundary conditions of the plate.

examples on heat conduction and solid mechanics problems are given in the following based on the computation using the developed code. The first one is compared to the available analytical solution, and the remaining ones are compared with results from the FEM software ANSYS or the published method EDM in reference [47,48]. The first two examples are for 2D and the last two

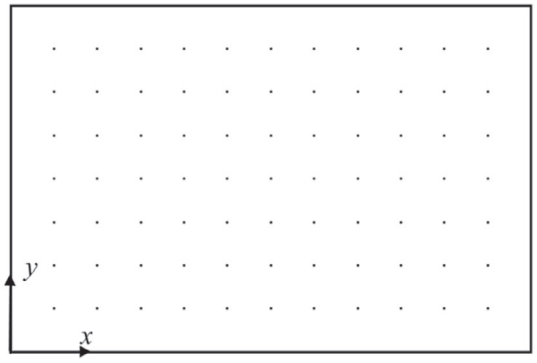

(a) Regular model of 13×9 nodes

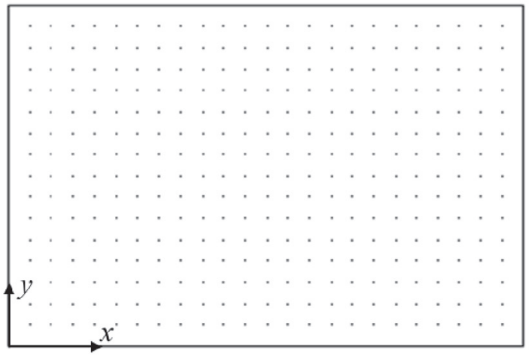

(b) Regular model of 25×17 nodes

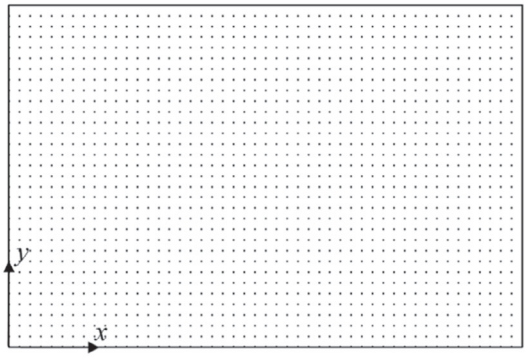

(c) Regular model of 49×33 nodes

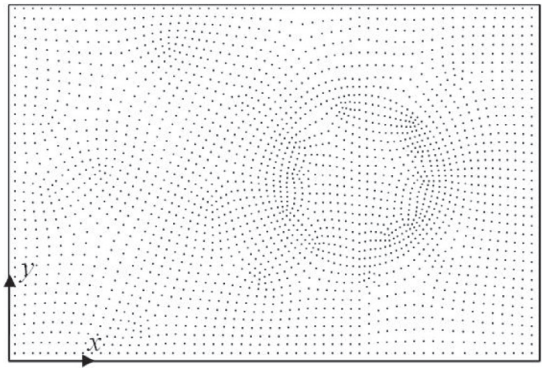

(d) Irregular model with total of 2517 nodes

Fig. 7. Nodes used in FECM analysis of the plate.

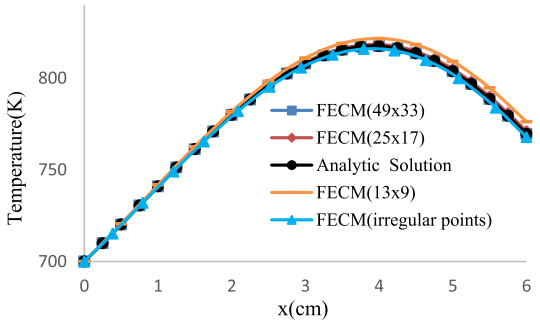

Fig. 8. Temperature distribution along horizontal direction.

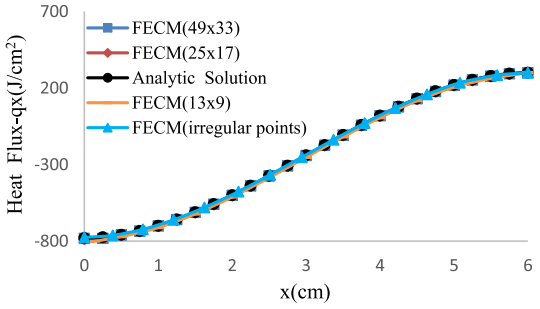

Fig. 9. Heat flux vector distribution along horizontal direction.

Table 1
Temperature (K) along x-direction.

x	FECM	Analytic	Error (%)
0.0	700.0000	700.0000	0.0000
0.5	720.2726	720.1440	0.0178
1.0	741.1464	740.8809	0.0358
1.5	761.5344	761.1221	0.0542
2.0	780.3167	779.7480	0.0729
2.5	796.3793	795.6470	0.0920
3.0	808.6639	807.7583	0.1121
3.5	816.2330	815.1465	0.1333
4.0	818.3510	817.0762	0.1560
4.5	814.5863	813.1172	0.1807
5.0	804.9374	803.2700	0.2076
5.5	789.9872	788.1162	0.2374
6.0	771.0905	769.0151	0.2699

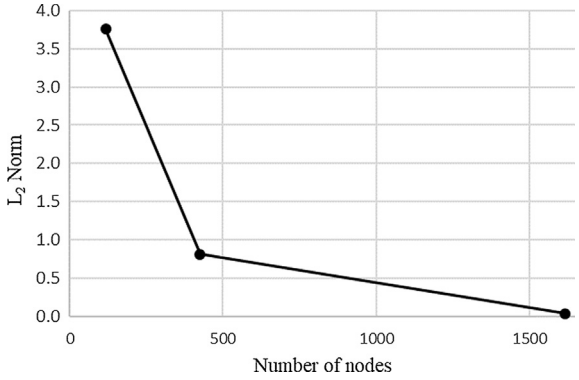

Fig. 10. The curve of L_2 norm versus the number of nodes.

Please cite this article as: X.-W. Gao, L. F. Gao, Y. Zhang et al., Free element collocation method: A new method combining advantages of finite element and mesh free methods, Computers and Structures, https://doi.org/10.1016/j.compstruc.2019.02.002

Table 2
Condition numbers for different models.

Model	No. of nodes	Condition number
13x9	117	4.7428E+03
25x17	425	3.4012E+04
49x33	1617	2.5677E+05
Irregular	2517	8.9004E+05

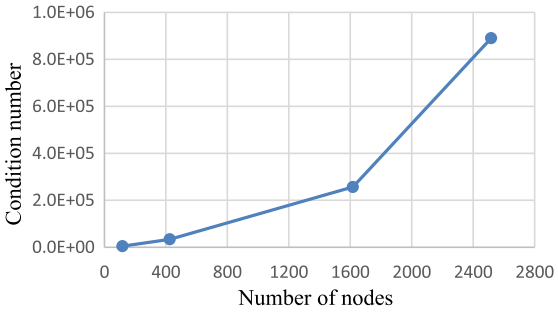

Fig. 11. Variation of condition number with number of nodes.

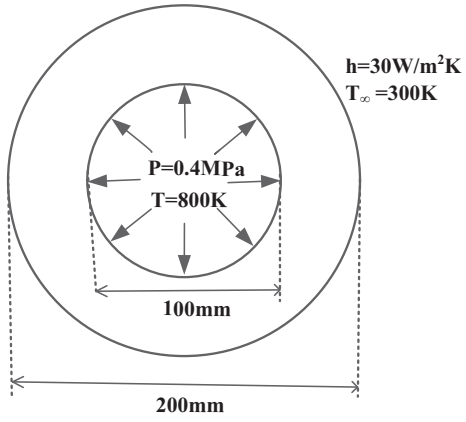

Fig. 12. Thick cylinder under thermal load and internal pressure.

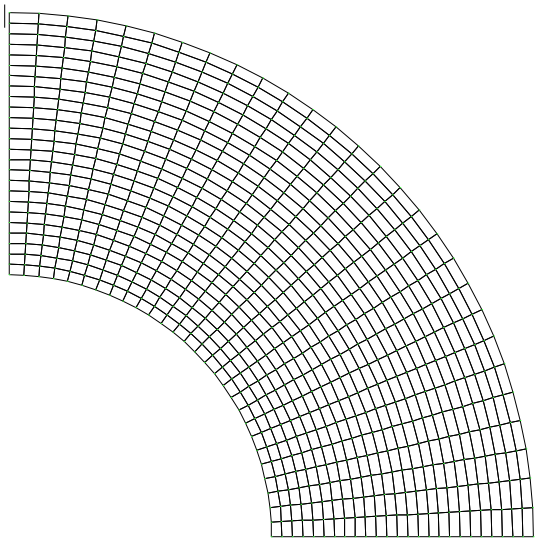

Fig. 13. Computational mesh used in EDM analysis.

are for 3D problems. To investigate the mesh-convergence behavior of the proposed method, which is very important [27,28] for a strong-form collocation method like FECM to examine its stability, three of the four examples are computed using different models with different numbers of computational nodes. All examples are computed on the ThinkPad Laptop computer with the i7-6600U CPU of 2.81 GHz and RAM of 16 GB.

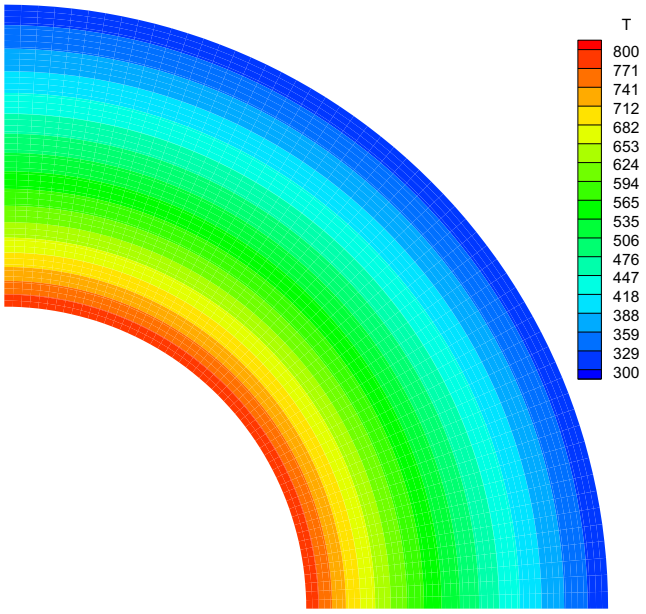

Fig. 14. Contour plot of the computed temperature over the cylinder.

Table 3
Temperature distribution along radial direction.

r	EDM	FECM	Error (%)
50.000000	800.000000	800.000000	0
55.000000	731.888306	731.899353	0.001509
60.000000	669.711853	669.729370	0.002616
65.000000	612.518860	612.539429	0.003358
70.000000	559.569214	559.590515	0.003807
75.000000	510.276672	510.296844	0.003953
80.000000	464.168518	464.186310	0.003833
85.000000	420.858215	420.872589	0.003415
90.000000	380.025543	380.035828	0.002706
95.000000	341.402374	341.407990	0.001645
100.000000	304.761810	304.762482	0.00022

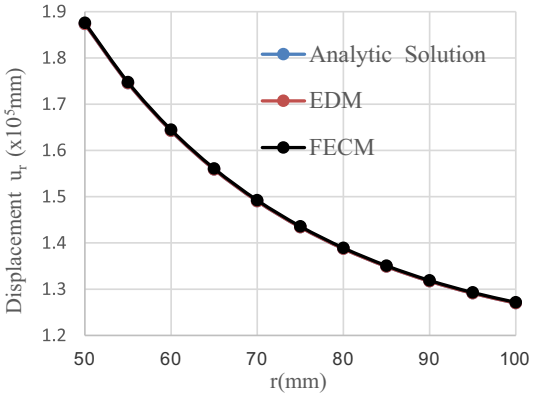

Fig. 15. Computed radial displacement u_r along radial direction.

Please cite this article as: X.-W. Gao, L. F. Gao, Y. Zhang et al., Free element collocation method: A new method combining advantages of finite element and mesh free methods, Computers and Structures, https://doi.org/10.1016/j.compstruc.2019.02.002

6.1. Example 1 – Heat conduction over a rectangular plate with varying conductivity and heat source

The first example considered is a plate of 6cm×4cm with the varying conductivity and heat source along x-direction (horizontal direction) as follows:

$$\lambda_{ij}(\boldsymbol{x}) = \lambda(\boldsymbol{x})\delta_{ij} \quad \text{with} \quad \lambda(\boldsymbol{x}) = 20e^{-x/6}, \quad Q(\boldsymbol{x}) = 30x(6-x)$$

The top and bottom sides of the plate are insulated, while the left and right sides are imposed with the temperature condition of 700 °C and the flux condition of 300 J/cm^2·s, respectively. Fig. 6 shows the dimension and boundary conditions of the plate. Three nodes-uniformly-distributed FECM models with different numbers of nodes along horizontal and vertical directions are used as shown in the first three figures in Fig. 7, in which the numbers of nodes are 13 × 9 = 117, 25 × 17 = 425 and 49 × 33 = 1617, respectively. To examine the impact of the point placement on the accuracy, a computational model with irregularly distributed nodes is also used in this example as shown in Fig. 7(d). For each node, the 9-node quadrilateral isoparametric element as shown in Fig. 1 is locally formed with the surround nodes.

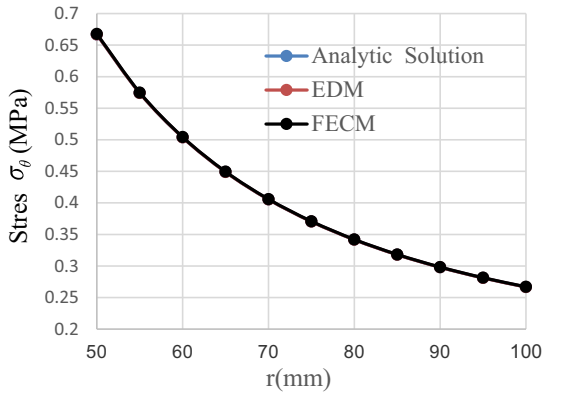

(a) Circumferential stress σ_θ

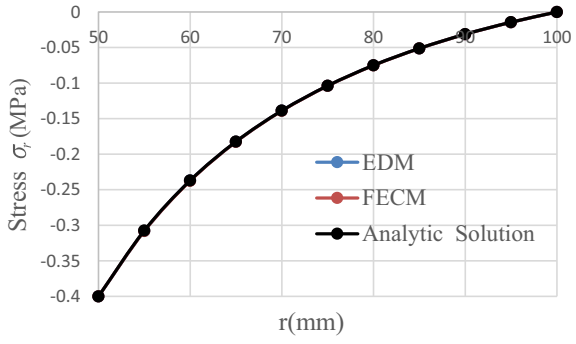

(b) The radial stress σ_r

Fig. 16. Computed circumferential and radial stresses along radial direction.

This problem actually is a one-dimensional heat conduction problem, for which the analytical solutions to the temperature and heat flux vector q_x (with $q_x = -\lambda\partial T/\partial x$) can be easily derived as follows:

$$T = e^{x/6}(3x^3 - 81x^2 + 972x - 5598) + 6298$$
$$q_x = 90x^2 - 10x^3 - 780$$

Figs. 8 and 9 give the distributions of the computed temperature T and flux vector q_x along the middle line of the plate. To have a detailed examination, Table 1 lists the value of temperature at different position based on the computational model of 25 × 17 nodes. For comparison purpose, the analytical solution is also given there. From Figs. 8 and 9, it can be seen that the FECM results are in good agreement with the analytical solution, and Table 1 shows that the maximum relative error of the computed temperature is less than 1%. This indicates that the proposed method is correct. A surprising phenomenon on observing Figs. 8 and 9 is that the mesh convergence behavior, which embodies the stability of the computational method, of the heat flux vector is even better than the temperature. Besides, the computed heat flux on the left side (x = 0) is, respectively, −788.346, −782.142 and −780.611 from the three coarse-to-fine models, which gradually approach the analytical value of −780.000 and this quantificationally confirms the correctness and convergence of the computed heat flux. To examine the global convergence of the computed results to the number of nodes, the L_2-norm over the entire domain nodes are 3.76E+00, 8.12E−01 and 3.45E−02 for the three coarse-to-fine models, respectively, which is also drawn in Fig. 10 and defined as $L_2 = \sqrt{(\boldsymbol{T}-\bar{\boldsymbol{T}})\cdot(\boldsymbol{T}-\bar{\boldsymbol{T}})/n}$ where $\boldsymbol{T}$ and $\bar{\boldsymbol{T}}$ are the computed temperature vector and analytical solution vector at all nodes, with n being the number of total nodes. The values and the diminution speed of L_2–norm indicate that the good accuracy can be achieved for all nodes and proper boundary conditions are set for all models. On the other hand, from Figs. 8 and 9, it can be seen that an increasing error from one side to the other can be observed in the results of the coarse mesh model (the model of 13 × 9 nodes). This might be because the system of Eq. (28) is expressed in terms of temperature and the left side of the example is specified with the temperature itself. When the finer nodes are used (the other two models), the computed results are in good agreement with analytical ones.

To examine the impact of the point placement on the condition number of the system matrix, Table 2 lists the condition numbers for the four computational models and Fig. 11 shows the variation of the condition number C_n with the number of nodes, which is

Table 4
Computed results along r-direction.

r (mm)	u_r-Analytic (×10^{-5} mm)	u_r-FECM (×10^{-5} mm)	σ_θ-Analytic (MPa)	σ_θ-FECM (MPa)	σ_r-Analytic (MPa)	σ_r-FECM (MPa)
50.	1.873016	1.875602	0.666667	0.667770	−0.400000	−0.400000
55.	1.745166	1.747569	0.574105	0.574827	−0.307438	−0.308105
60.	1.642328	1.644581	0.503704	0.504341	−0.237037	−0.237551
65.	1.55873	1.560859	0.448915	0.449485	−0.182248	−0.182650
70.	1.490249	1.492275	0.405442	0.405957	−0.138775	−0.139090
75.	1.433862	1.435801	0.37037	0.370840	−0.103703	−0.103951
80.	1.387301	1.389167	0.341667	0.342099	−0.075000	−0.075193
85.	1.348833	1.350637	0.317878	0.318279	−0.051211	−0.051361
90.	1.317108	1.318860	0.297942	0.298317	−0.031276	−0.031389
95.	1.291061	1.292770	0.281071	0.281423	−0.014404	−0.014488
100.	1.269841	1.271513	0.266667	0.267014	0.000000	0.000000

Please cite this article as: X.-W. Gao, L. F. Gao, Y. Zhang et al., Free element collocation method: A new method combining advantages of finite element and mesh free methods, Computers and Structures, https://doi.org/10.1016/j.compstruc.2019.02.002

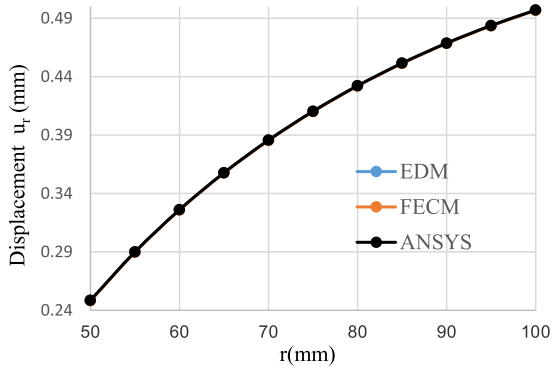

Fig. 17. Distribution of displacement u_r under thermal and elastic loading.

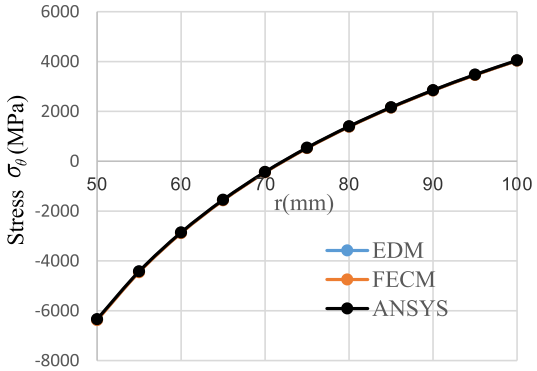

Fig. 18. Distribution of circumferential stress under thermal and elastic loading.

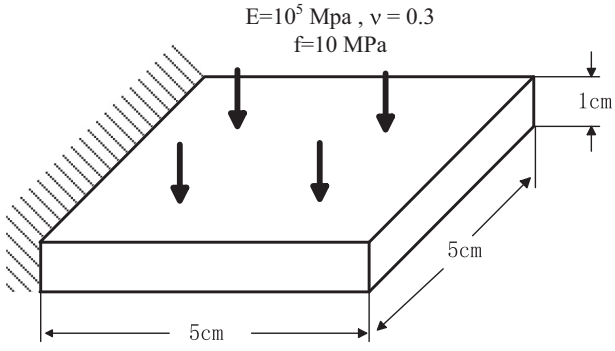

Fig. 19. A thick plate under the bending load.

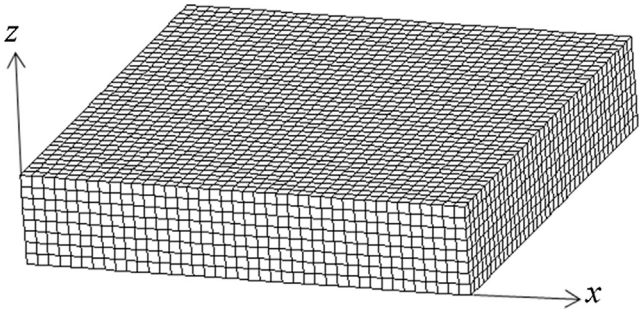

Fig. 20. Global view of the overlapped free elements in FECM analysis.

defined as $C_n = \| K \| \cdot \| K^{-1} \|$ where K is the coefficient matrix in Eq. (28) and $\| K \| = \left(\sum_{i=1}^{N} \sum_{j=1}^{N} K_{ij}^2 \right)^{1/2}$ with N being the number of lines and columns in matrix K.

From Figs. 8 and 9 it can be seen that even for the irregular model, the result is in good agreement with the analytical one. This indicates that the impact of point placement on accuracy is not large. On the other hand, Table 2 and Fig. 11 show that the point placement has some influence on the condition number of the system matrix, but it is still in the health region.

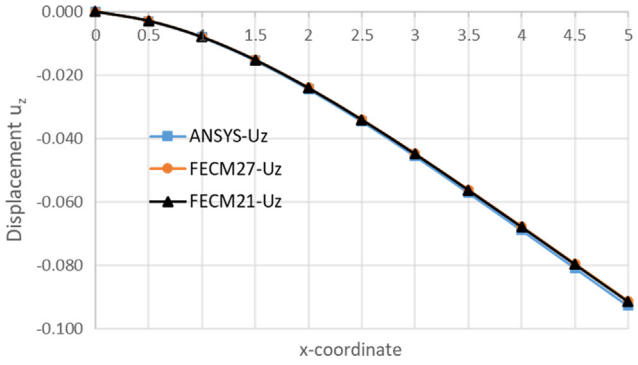

Fig. 21. Displacements u_z computed using ANSYS and FECM.

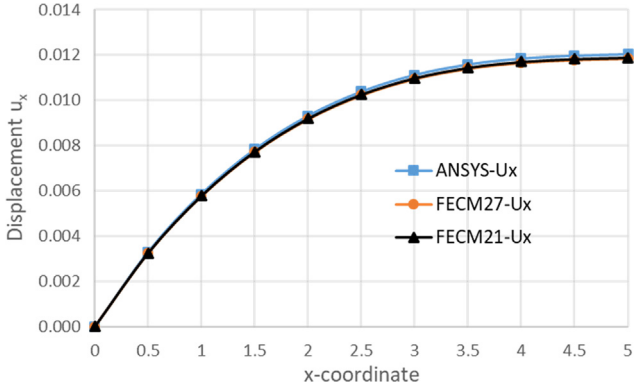

Fig. 22. Displacement u_x computed using ANSYS and FECM.

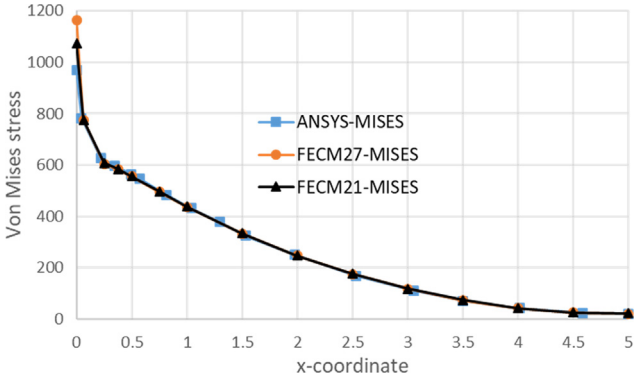

Fig. 23. Von Mises stress computed using ANSYS and FECM.

Please cite this article as: X.-W. Gao, L. F. Gao, Y. Zhang et al., Free element collocation method: A new method combining advantages of finite element and mesh free methods, Computers and Structures, https://doi.org/10.1016/j.compstruc.2019.02.002

6.2. Example 2: Thick-walled cylinder under thermal load and internal pressure

The second example deals with a thick-walled cylinder with an inner and outer diameters of 100 mm and 200 mm (see Fig. 12). The inner surface of the cylinder is subjected to a pressure of P = 0.4 MPa and a temperature boundary condition of 800 K, and the outer surface is traction free and lying in an heat convective environment of $h = 30$ W/m^2·K and $T_\infty = 300$ K. The material properties of the cylinder are: heat conductivity $\lambda = 20$ W/m·K, elastic modules $E = 2.1 \times 10^6$ and Poisson's ratio $\nu = 0.3$. The heat conduction, elasticity, and thermoelasticity analyses are performed for the cylinder. In the conduction analysis, no heat source is considered, and in the elasticity analysis, the plane stress condition is considered.

Due to symmetry, a quarter of the cylinder is analyzed. For comparison, the problem is also computed using EDM proposed in Refs. [47,48]. In the EDM analysis, the model is discretized into 700 nigh-node Lagrange elements with 2907 nodes (see Fig. 13). In the present FECM analysis, the same nodes are used as in EDM, but each node uses one 9-node Lagrange element freely formed with around nodes. The final pattern of the overlapped free elements for all nodes is similar to Fig. 13.

6.2.1. Temperature computation

Firstly, the heat conduction computation is performed to determine the temperature field by applying the temperature and convective boundary conditions as shown in Fig. 12. Fig. 14 is the contour plot of the temperature computed using FECM, while Table 3 lists the temperature distribution along the radial direction. It can be seen that the temperature computed using FECM is very close to that using EDM. The maximum relative error between two methods is within 0.01%.

6.2.2. Elasticity computation

Secondly, the problem is computed under elasticity plane stress condition using the same geometry and discretization as the previous thermal case. The boundary conditions are shown in Fig. 12,

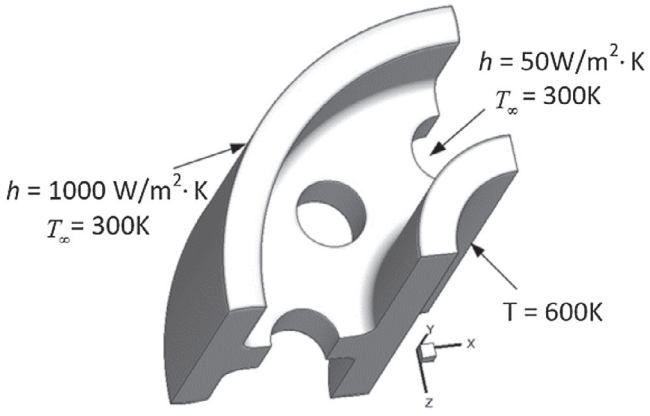

(a) A quarter of the belt wheel

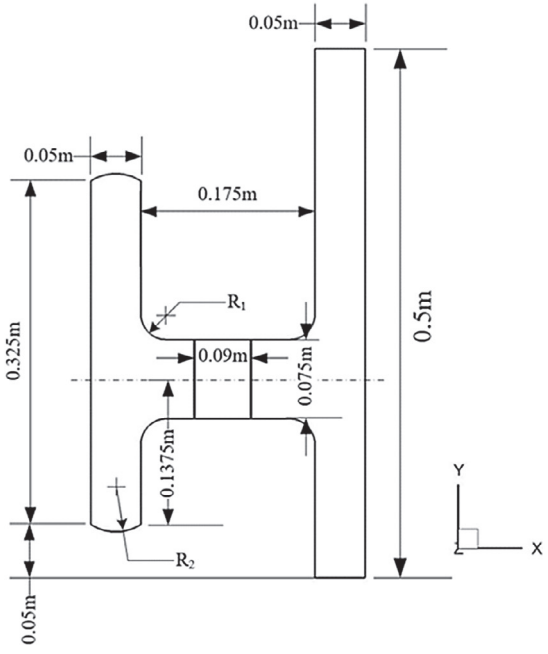

(b) Front view of a vertical plane

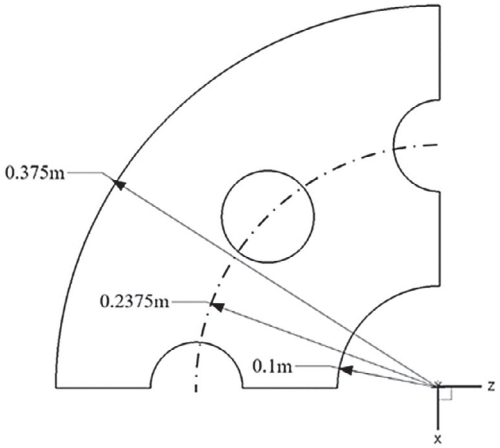

(c) Overlook of the meddle plane

Fig. 24. A belt wheel under thermal environment.

Please cite this article as: X.-W. Gao, L. F. Gao, Y. Zhang et al., Free element collocation method: A new method combining advantages of finite element and mesh free methods, Computers and Structures, https://doi.org/10.1016/j.compstruc.2019.02.002

subjected to a pressure of P = 0.4 MPa on the inner surface of the cylinder. In this computation, the temperature change is taken as zero. Figs. 15 and 16 show the distributions of the computed radial displacement u_r, and the circumferential and radial stresses σ_θ and σ_r along the radial direction of the cylinder. For a clear insight of the computational accuracy, Table 4 lists the detailed values of u_r, σ_θ and σ_r at different values of r. For this computation, the analytical solutions are available [54], which are

$$u_r = \frac{1}{E}\frac{a^2P}{b^2-a^2}[(1+v)\frac{b^2}{r}+(1-v)r]$$

$$\sigma_\theta = \frac{a^2}{b^2-a^2}(1+\frac{b^2}{r^2})P, \quad \sigma_r = \frac{a^2}{b^2-a^2}(1-\frac{b^2}{r^2})P$$

where a and b are the inner and outer radius of the cylinder.

For comparison, these analytical solutions are also plotted in these figures. From Figs. 15 and 16 as well as Table 4, it can be seen that the present FECM results are in good agreement with the EDM results. This indicates that the proposed method is correct for the elasticity analysis.

6.2.3. Thermoelasticity computation

Finally, the cylinder is simulated under the thermal and mechanical loads as shown in Fig. 12. In the computation, the temperature field shown in Fig. 14 is taken as the temperature change used in Eqs. (24), (27) and (30). Figs. 17 and 18 show the distributions of the computed radial displacement u_r and circumferential stress σ_θ along the radial direction of the cylinder. For this computation, since no analytical results are available, the results computed using the FEM software ANSYS are plotted in Figs. 17 and 18 for comparison. It can be seen that the results computed using FECM, EDM and ANSYS are very close. On the other hand, contracting Figs. 17 and 18 with Figs. 15 and 16, it can be seen that the displacement and stress under the thermal loading are much larger than that under the pure mechanical load. Even the trends of change are totally different. This indicates that under high temperature field, the thermal stress may be the main reason causing structure failure.

6.3. Example 3: Thick plate subjected to a bending load

The third example is concerned with a 3D thick plate with the Young's modulus of $E = 10^5$ MPa and Poisson ratio of $v = 0.3$ under a uniformly distributed bending load $\boldsymbol{f} = 10$ MPa on the top surface. The dimensions of the plate are shown in Fig. 19. The left side of the plate is fixed. In the FECM computation, the plate is discretized into 63,257 nodes. Each node is analyzed using one free element formed by around nodes. For validation and comparison, two computations are performed in FECM by using 27-node and 21-node free elements, respectively, as shown in Figs. 2 and 3. All formed free elements for all nodes constitute an overlapped mesh as shown in Fig. 20.

To validate the correctness of FECM, the problem is also computed using the FEM software ANSYS with a finer model of 25,000 Solid186 elements and 110,721 nodes. Figs. 21 and 22 give the distributions of the computed displacements u_z and u_x along the middle line of the top surface of the plate, while Fig. 23 is a plot of the computed Von Mises stresses [64], in which FECM27 and FECM21mean the results computed using the 27-node and 21-node free elements, respectively.

From Figs. 21–23 it can be seen that the computed results using current FECM are very close to the results using ANSYS. This further validates the correctness of the proposed method in the paper. On the other hand, Fig. 23 shows that the Von Mises stress computed using both the 27-node and the 21-node free elements have an excellent agreement with the result using ANSYS except for the fixed side of $x = 0$ where the stress concentration occurs and no a certain exact result exists.

6.4. Example 4: Thermal analysis of a belt wheel

The forth example is on the thermal analysis of a belt wheel, a quarter of which is shown in Fig. 24. The all surfaces of the wheel are exposed in an environment of $T_\infty = 300$ Kexcept for the inter one where the temperature of $T = 600$ K is imposed. The heat transfer coefficient is $h = 50$ W/m^2·K on the small hole surfaces and $h = 1000$ W/m^2·K on the outer surface of the wheel. The heat conductivity of the wheel material is $\lambda = 700$ W/m·K. The heat conduction computation under these conditions is performed using three different models, which have the numbers of nodes of 381855,

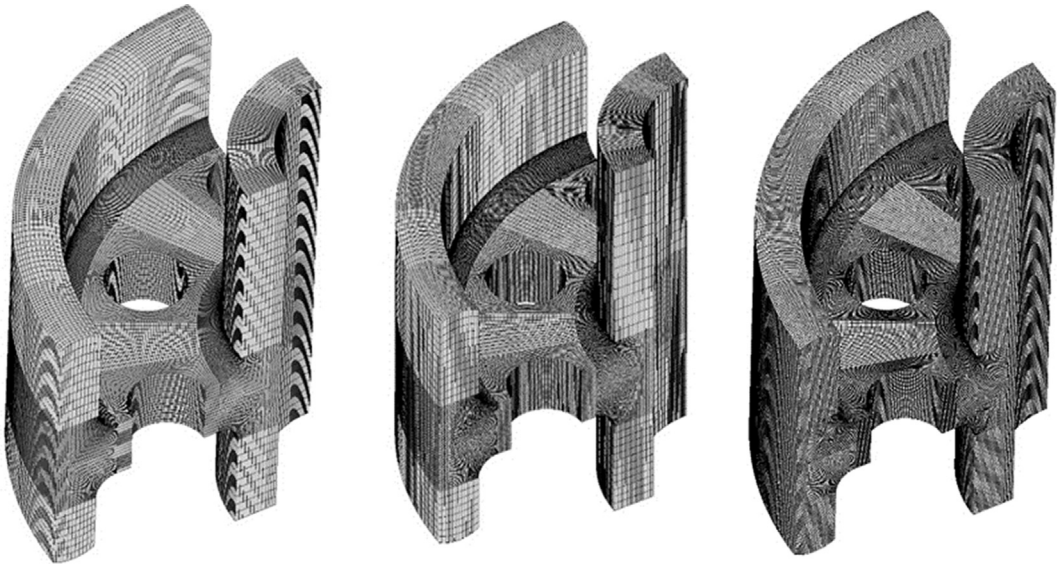

Fig. 25. Three computational models of the belt wheel.

Please cite this article as: X.-W. Gao, L. F. Gao, Y. Zhang et al., Free element collocation method: A new method combining advantages of finite element and mesh free methods, Computers and Structures, https://doi.org/10.1016/j.compstruc.2019.02.002

835,234 and 1880380, respectively, and are shown in Fig. 25 for the overlapped meshes of all locally formed 21-node collocation elements. Fig. 26 shows the contour of the computed temperature T and flux magnitude q which is defined as $q = \sqrt{q_x^2 + q_y^2 + q_z^2}$ with $q_x = -\lambda \partial T/\partial x$. Fig. 27 shows the distribution of the computed temperature along line AB. Table 5 lists the detailed values of the temperature computed using the model of 1,880,380 nodes. For comparison, the results from ANSYS with the same number and distribution of the nodes are also listed there. From Table 5 it can be seen that the current results are in excellent agreement with the ANSYS results. On the other hand, from Fig. 27, it can be seen that the mesh-convergence is very good for the three computational models used in FECM. A small discrepancy can be observed for the coarse mesh of 381,855 nodes. The results of other two models are almost the same as that of ANSYS.

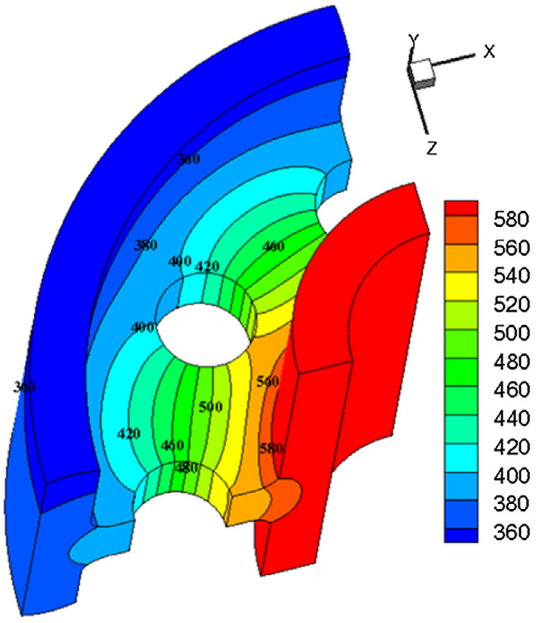

(a) Contour plot of the computed temperature

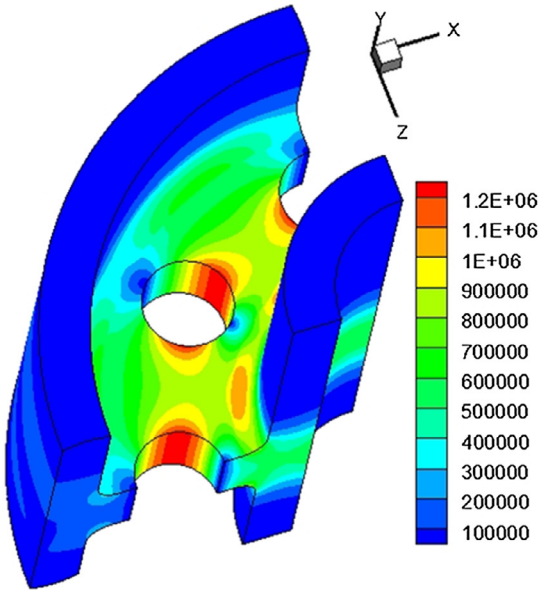

(b) Contour plot of the computed flux magnitude

Fig. 26. Contour plot of the computed temperature and flux magnitude.

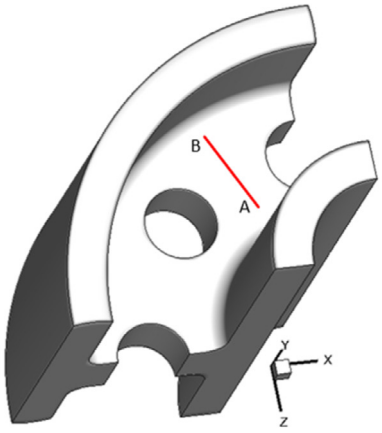

(a) Line AB to be tabulated

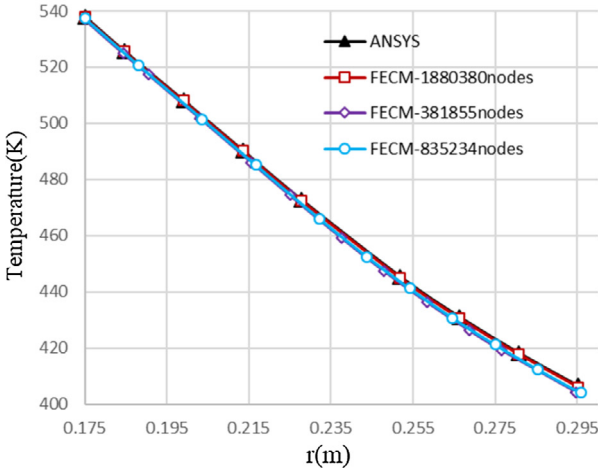

(b) Temperature distribution along line AB

Fig. 27. Comparison of the computed temperature along line AB.

Table 5
Computed temperature along line AB (r-direction).

r	T_{ANSYS}	$T_{FECM1880380}$	Error (%)
0.175001152	537.88	537.8489	0.00578
0.184613095	525.65	525.612	0.00723
0.199040822	508.08	507.9986	0.016
0.213458927	490.34	490.178	0.03
0.227886654	472.67	472.4099	0.055
0.251926323	445.32	444.8868	0.0973
0.266345959	430.96	430.4716	0.113
0.280773686	418.19	417.6694	0.124
0.295192174	406.53	405.9937	0.132

6.5. Computational time

The method proposed in this paper is based on the element differential formulation derived in EDM [48]. To examine the computational efficiency between FECM and EDM, the computational time spent in the above last two (3D) examples are listed in Table 6.

Please cite this article as: X.-W. Gao, L. F. Gao, Y. Zhang et al., Free element collocation method: A new method combining advantages of finite element and mesh free methods, Computers and Structures, https://doi.org/10.1016/j.compstruc.2019.02.002

Table 6
Computational time spent by FECM and EDM in the last two examples.

	Used method	forming coefficient	solving system of equations	total time
Example 3 (111,537 nodes)	EDM	37 s	166 s	203 s
	FECM	17 s	118 s	135 s
Example 4 (1,880,380 nodes)	EDM	8242 s	1481	9723 s
	FECM	7457 s	1195 s	8652 s

The time spent in the first two (2D) examples is almost zero, so it is not listed here.

From Table 6 it can be seen that the spent times by FECM are less than EDM both in forming the coefficient $\boldsymbol{K}$ in Eq. (28) (being $\boldsymbol{A}$ in EDM [48]) and in solving the final system of equations. This is attributed to the fact that only one collocation element is used at each node in FECM, which not only can reduce the number of collocation elements from 8 to 1 (in general cases) for each collocation node, but also can decrease the bandwidth of the system of equations considerably, so that the individual and total computational times can be correspondingly saved.

7. Concluding discussions

A new numerical method, free element collocation method (FECM), has been proposed in this paper for solving general second order PDEs based on the use of isoparametric elements. The following conclusions and discussions can be drawn:

(1) FECM is a strong-form technique, which belongs to the category of the mesh free method (MFM) and works based on the elements of FEM.
(2) FECM is a type of point collocation method (PCM), which forms the system of equations node by node. It has the advantage of easy use as in PCM, and the advantage of easily generating meshes (elements) as in MFM, and the advantage of being able to achieve stable results as in the standard FEM.
(3) Since FECM uses the isoparametric elements to model the geometry and represent physical variables, the shape functions of the used elements have the Delta symbol characteristic, so that the boundary conditions can be directly imposed on the system of equations, being able to overcome the difficulty existing in the general MFM.
(4) The final system of equations formed in FECM is not symmetric, but attributing to the use of only one element at each node, the bandwidth of the system coefficient matrix is extremely narrow, such that the computational efficiency of FECM can be very high.
(5) As discussed in [65,66] on isogeometric analysis, the local adaptive ability is important for the geometry independent field approximation. Attributing to the feature that the individual element for each point can be independently and freely formed, FECM has excellent local adaptive ability in refining points locally. Moreover, by using the nodes-non-equally-spaced Lagrange elements, stable results can be obtained by FECM even using models with irregularly distributed points. These have been verified by example 1 by using one model with irregular points and example 4 where many places have non-uniformly distributed points.

Acknowledgments

The support of this investigation by the National Natural Science Foundation of China under Grant Nos. 11672061, 11702054, 51576026 is gratefully acknowledged.

Appendix:. Shape functions for the 21-node hexahedron element shown in Fig. 3

$$N_1(\xi,\eta,\zeta)=\tfrac{1}{24}\{-(-3+\xi)\xi+3\zeta(-1+\eta)(-1+\xi)(1+\eta+\xi)-3\eta(-1+\xi^2)+\eta^2(-1+\xi(-3+2\xi))+\zeta^2(-1+2\eta^2+3\eta(-1+\xi)+\xi(-3+2\xi))\}$$

$$N_2(\xi,\eta,\zeta)=\tfrac{1}{24}\{-3\zeta(-1+\eta)(1+\eta-\xi)(1+\xi)-\xi(3+\xi)-3\eta(-1+\xi^2)+\eta^2(-1+\xi(3+2\xi))+\zeta^2(-1+2\eta^2-3\eta(1+\xi)+\xi(3+2\xi))\}$$

$$N_3(\xi,\eta,\zeta)=\tfrac{1}{24}\{-\xi(3+\xi)-3\zeta(1+\eta)(1+\xi)(-1+\eta+\xi)+3\eta(-1+\xi^2)+\eta^2(-1+\xi(3+2\xi))+\zeta^2(-1+2\eta^2+3\eta(1+\xi)+\xi(3+2\xi))\}$$

$$N_4(\xi,\eta,\zeta)=\tfrac{1}{24}\{-\eta(3+\eta)+3\zeta(1+\eta)(-1+\eta-\xi)(-1+\xi)-3(-1+\eta^2)\xi+(-1+\eta(3+2\eta))\xi^2+\zeta^2(-1+3\eta+2\eta^2-3(1+\eta)\xi+2\xi^2)\}$$

$$N_5(\xi,\eta,\zeta)=\tfrac{1}{24}\{-(-3+\xi)\xi-3\zeta(-1+\eta)(-1+\xi)(1+\eta+\xi)-3\eta(-1+\xi^2)+\eta^2(-1+\xi(-3+2\xi))+\zeta^2(-1+2\eta^2+3\eta(-1+\xi)+\xi(-3+2\xi))\}$$

$$N_6(\xi,\eta,\zeta)=\tfrac{1}{24}\{3\zeta(-1+\eta)(1+\eta-\xi)(1+\xi)-\xi(3+\xi)-3\eta(-1+\xi^2)+\eta^2(-1+\xi(3+2\xi))+\zeta^2(-1+2\eta^2-3\eta(1+\xi)+\xi(3+2\xi))\}$$

$$N_7(\xi,\eta,\zeta)=\frac{1}{24}\{-\xi(3+\xi)+3\zeta(1+\eta)(1+\xi)(-1+\eta+\xi)+3\eta(-1+\xi^2)+\eta^2(-1+\xi(3+2\xi))+\zeta^2(-1+2\eta^2+3\eta(1+\xi)+\xi(3+2\xi))\}$$

$$N_8(\xi,\eta,\zeta)=\tfrac{1}{24}\{-\eta(3+\eta)-3(-1+\eta^2)\xi+(-1+\eta(3+2\eta))\xi^2+3\zeta(1+\eta)(-1+\xi)(1-\eta+\xi)+\zeta^2(-1+3\eta+2\eta^2-3(1+\eta)\xi+2\xi^2)\}$$

$$N_9(\xi,\eta,\zeta)=\frac{1}{12}\{\eta(-3+2\eta)-(1+(-3+\eta)\eta)\xi^2-3\zeta(-1+\eta)(-1+\xi^2)-\zeta^2(-2+\eta^2+\xi^2)\}$$

$$N_{10}(\xi,\eta,\zeta)=\frac{1}{12}\{3\zeta(-1+\eta^2)(1+\xi)+\xi(3+2\xi)-\zeta^2(-2+\eta^2+\xi^2)-\eta^2(1+\xi(3+\xi))\}$$

$$N_{11}(\xi,\eta,\zeta)=\frac{1}{12}\{\eta(3+2\eta)-(1+\eta(3+\eta))\xi^2+3\zeta(1+\eta)(-1+\xi^2)-\zeta^2(-2+\eta^2+\xi^2)\}$$

$$N_{12}(\xi,\eta,\zeta)=\frac{1}{12}\{-3\zeta(-1+\eta^2)(-1+\xi)+\xi(-3+2\xi)-\eta^2(1+(-3+\xi)\xi)-\zeta^2(-2+\eta^2+\xi^2)\}N_{13}(\xi,\eta,\zeta)$$
$$=\frac{1}{12}\{\eta(-3+2\eta)-(1+(-3+\eta)\eta)\xi^2+3\zeta(-1+\eta)(-1+\xi^2)-\zeta^2(-2+\eta^2+\xi^2)\}N_{14}(\xi,\eta,\zeta)$$
$$=\frac{1}{12}\{-3\zeta(-1+\eta^2)(1+\xi)+\xi(3+2\xi)-\zeta^2(-2+\eta^2+\xi^2)-\eta^2(1+\xi(3+\xi))\}$$

$$N_{15}(\xi,\eta,\zeta)=\frac{1}{12}\{\eta(3+2\eta)-(1+\eta(3+\eta))\xi^2-3\zeta(1+\eta)(-1+\xi^2)-\zeta^2(-2+\eta^2+\xi^2)\}$$

Please cite this article as: X.-W. Gao, L. F. Gao, Y. Zhang et al., Free element collocation method: A new method combining advantages of finite element and mesh free methods, Computers and Structures, https://doi.org/10.1016/j.compstruc.2019.02.002

$$N_{16}(\xi,\eta,\zeta)=\frac{1}{12}\{3\zeta(-1+\eta^2)(-1+\xi)+\xi(-3+2\xi)-\eta^2(1+(-3+\xi)\xi)-\zeta^2(-2+\eta^2+\xi^2)\}$$

$$N_{17}(\xi,\eta,\zeta)=\frac{1}{12}\{3\eta(-1+\xi)+\xi(-3+2\xi)-\zeta^2(1+\eta^2+3\eta(-1+\xi)+(-3+\xi)\xi)-\eta^2(-2+\xi^2)\}$$

$$N_{18}(\xi,\eta,\zeta)=\frac{1}{12}\{-3\eta(1+\xi)+\xi(3+2\xi)-\eta^2(-2+\xi^2)-\zeta^2(1+\eta^2-3\eta(1+\xi)+\xi(3+\xi))\}$$

$$N_{19}(\xi,\eta,\zeta)=\frac{1}{12}\{3\eta(1+\xi)+\xi(3+2\xi)-\eta^2(-2+\xi^2)-\zeta^2(1+\eta^2+3\eta(1+\xi)+\xi(3+\xi))\}$$

$$N_{20}(\xi,\eta,\zeta)=\frac{1}{12}\{\eta(3+2\eta)-3(1+\eta)\xi-(-2+\eta^2)\xi^2-\zeta^2(1+3\eta+\eta^2-3(1+\eta)\xi+\xi^2)\}$$

$$N_{21}(\xi,\eta,\zeta)=\frac{1}{3}\{3-2\xi^2+\eta^2(-2+\xi^2)+\zeta^2(-2+\eta^2+\xi^2)\}$$

References

[1] Zienkiewicz OC, Taylor RL. The finite element method. 6th ed. UK: Butterworth-Heinemann; 2005. vol. 2.
[2] Hughes TJR. The finite element method: linear static and dynamic finite element analysis. New Jersey, USA: Prentice-Hall; 1987.
[3] Tao WQ, He YL, Wang QW, Qu ZG, Song FQ. A unified analysis on enhancing single phase convective heat transfer with field synergy principle. Int J Heat Mass Transf 2002;45(24):4871–9.
[4] Lee CH, Gil AJ, Bonet J. Development of a cell centred upwind finite volume algorithm for a new conservation law formulation in structural dynamics. Comput Struct 2013;118:13–38.
[5] Li J, Peterson GP, Cheng P. Dynamic characteristics of transient boiling on a square platinum microheater under millisecond pulsed heating. Int J Heat Mass Transfer 2008;51(1):273–82.
[6] Chen Z, Huan G, Ma Y. Computational methods for multiphase flows in porous media; 2006.
[7] Jensen PS. Finite difference techniques for variable grids. Comput Struct 1972;2(1–2):17–29.
[8] Liszka T, Orkisz J. The finite difference method at arbitrary irregular grids and its application in applied mechanics. Comput Struct 1980;11(1–2):83–95.
[9] Liu GR, Zhang J, Li H, Lam KY, Kee BBT. Radial point interpolation based finite difference method for mechanics problems. Int J Numer Meth Eng 2006;68(7):728–54.
[10] Cui M, Duan WW, Gao XW. A new inverse analysis method based on a relaxation factor optimization technique for solving transient nonlinear inverse heat conduction problems. Int J Heat Mass Transfer 2015;90:491–8.
[11] Han F, Dai W. New higher-order compact finite difference schemes for 1D heat conduction equations. Appl Math Model 2013;37(16–17):7940–52.
[12] Brebbia CA, Telles JC, Wrobel LC. Boundary element techniques. Berlin: Springer; 1984.
[13] Divo E, Kassab AJ. Boundary element method for heat conduction: with applications in non-homogenous media. Southampton, UK: WIT Press; 2003.
[14] Sladeka V, Sladeka J, Tanakab M, Zhang C. Transient heat conduction in anisotropic and functionally graded media by local integral equations. Eng Anal Boundary Elem 2005;29(11):1047–65.
[15] Gao XW, Feng WZ, Zheng BJ, Yang K. An interface integral equation method for solving general multi-medium mechanics problems. Int J Numer Meth Eng 2016;107(8):696–720.
[16] Gao XW. A meshless BEM for isotropic heat conduction problems with heat generation and spatially varying conductivity. Int J Numer Meth Eng 2006;66(9):1411–31.
[17] Amiri F, Anitescu C, Arroyo M, Bordas SPA, Rabczuk T. XLME interpolants, a seamless bridge between XFEM and enriched meshless methods. Comput Mech 2014;53(1):45–57.
[18] Stéphane P, Bordas A, Natarajan S, Kerfriden P, Augarde CE, Mahapatra DR, et al. On the performance of strain smoothing for quadratic and enriched finite element approximations (XFEM/GFEM/PUFEM). Int J Numer Meth Eng 2011;86(4–5):637–66.
[19] Bordas SPA, Rabczuk T, Hung NX, Nguyen VP, Natarajan S, Bog T, et al. Strain smoothing in FEM and XFEM. Comput Struct 2010;88(23–24):1419–43.
[20] Hughes TJR, Cottrell JA, Bazilevs Y. Isogeometric analysis: CAD, finite elements, NURBS, exact geometry and mesh refinement. Comput Methods Appl Mech Eng 2005;194(39):4135–95.
[21] Auricchio F, Veiga LB, Buffa A, Lovadina C, Reali A, Sangalli G. A fully "locking-free" isogeometric approach for plane linear elasticity problems: a stream function formulation. Comput Methods Appl Mech Eng 2007;197(1):160–72.
[22] Sevilla R, Fernández-Méndez S, Huerta A. NURBS-enhanced finite element method (NEFEM). Int J Numer Meth Eng 2008;76:56–83.
[23] Schillinger D, Evans JA, Reali A, Scott MA, Hughes TJR. Isogeometric collocation: cost comparison with Galerkin methods and extension to adaptive hierarchical NURBS discretizations. Comput Methods Appl Mech Eng 2013;267:170–232.
[24] Peng X, Atroshchenko E, Kerfriden P, Bordas SPA. Linear elastic fracture simulation directly from CAD: 2d nurbs-based implementation and role of tip enrichment. Int J Fract 2017;204:55–78.
[25] Nguyen VP, Bordas SPA, Rabczuk T. Isogeometric analysis: an overview and computer implementation aspects. Math Comput Simul 2015;117:89–116.
[26] Simpson RN, Bordas SPA, Lian H, Trevelyan J. An isogeometric boundary element method for elastostatic analysis: 2D implementation aspects. Comput Struct 2013;118:2–12.
[27] Nguyen VP, Rabczuk T, Bordas S, Duflot M. Meshless methods: a review and computer implementation aspects. Math Comput Simul 2008;79(3):763–813.
[28] Liu GR. An overview on meshfree methods: for computational solid mechanics. Int J Comput Methods 2016;13(5):1630001.
[29] Zhang X, Liu XH, Song KZ, Lu MW. Least-square collocation meshless method. Int J Numer Meth Eng 2001;51(9):1089–100.
[30] Gu YT, Liu GR. A meshfree weak-strong (MWS) form method for time dependent problems. Comput Mech 2005;35(2):134–45.
[31] Wang D, Wu J. An efficient nesting sub-domain gradient smoothing integration algorithm with quadratic exactness for Galerkin meshfree methods. Comput Methods Appl Mech Eng 2016;298:485–519.
[32] Wang D, Zhang H. A consistently coupled isogeometric-meshfree method. Comput Methods Appl Mech Eng 2014;268:843–70.
[33] Wen PH, Aliabadi MH. An improved meshless collocation method for elastostatic and elastodynamic problems. Commun Numer Meth Eng 2008;24(8):635–51.
[34] Zheng BJ, Gao XW, Yang K, Zhang C. A novel meshless local Petrov-Galerkin method for dynamic coupled thermoelasticity analysis under thermal and mechanical shock loading. Eng Anal Boundary Elem 2015;60:154–61.
[35] Haq S, Hussain A, Uddin M. RBFs meshless method of lines for the numerical solution of time-dependent nonlinear coupled partial differential equations. Appl Math 2011;2(4):414–23.
[36] Khater AH, Temsah RS, Hassan MM. A chebyshev spectral collocation method for solving burgers' type equations. J Comput Appl Math 2008;222(2):333–50.
[37] Islam S, Haq S, Uddin M. A mesh free interpolation method for the numerical solution of the coupled nonlinear partial differential equations. Eng Anal Boundary Elem 2009;33(3):399–409.
[38] Uddin M, Haq S, Islam S. Numerical solution of complex modified kortewegde vries equation by mesh-Free collocation method. Comput Math Appl 2009;58(3):566–78.
[39] Bishay PL, Sladek J, Sladek V, Gao XW. Analysis of elastic media with voids using a mixed-collocation finite-element method (MCFEM). ASCE J Eng Mech 2017;143(4). 04016119-1-14.
[40] Zhang X, Sze KY, Ma S. An explicit material point finite element method for hyper velocity impact. Int J Numer Meth Eng 2006;66:689–706.
[41] Liu GR, Zhang J, Lam KY. A gradient smoothing method (GSM) with directional correction for solid mechanics problems. Comput Mech 2008;41:457–72.
[42] Sladek J, Stanak P, Han ZD, Sladek V, Atluri SN. Applications of the MLPG method in engineering & sciences: a review. CMES 2013;92(5):423–75.
[43] Yagawa G, Yamada T. Free mesh method: a new meshless finite element method. Comput Mech 1996;18:383–6.
[44] Yagawa G, Furukawa T. Recent developments approaches for accurate free mesh method. Int J Numer Meth Eng 2000;47:1445–62.
[45] Yagawa G, Matsubara H. Enriched element method and its applications to solid mechanics. Computational methods in engineering and science, EPMESC X, August 21–23, 2006, Sanya, Hainan, China.
[46] Kobayashi Y, Shioya R, Yagawa G. Parallel eigen frequency analysis using enriched free mesh method. Key Eng Mater 2011;462–463:628–33. ISSN: 1662-9795.
[47] Gao XW, Huang SZ, Cui M, Ruan B, Zhu QH, Yang K, et al. Element differential method for solving general heat conduction problems. Int J Heat Mass Transfer 2017;115:882–94.
[48] Gao XW, Li ZY, Yang K, Lv J, Peng HF, Cui M, et al. Element differential method and its application in thermal-mechanical problems. Int J Numer Meth Eng 2018;113(1):82–108.
[49] Wen PH, Cao P, Korakianitis T. Finite block method in elasticity. Eng Anal Boundary Elem 2014;46:116–25.
[50] Li M, Wen PH. Finite block method for transient heat conduction analysis in functionally graded media. Int J Numer Meth Eng 2014;99(5):372–90.
[51] Fantuzzi N, Tornabene F, Viola E, Ferreira AJM. A strong formulation finite element method (SFEM) based on RBF and GDQ techniques for the static and dynamic analyses of laminated plates of arbitrary shape. Meccanica 2014;49:2503–42.
[52] Fantuzzi N, Dimitri R, Tornabene F. A SFEM-based evaluation of mode-I Stress Intensity Factor in composite structures. Compos Struct 2016;145:162–85.
[53] Viola E, Tornabene F, Fantuzzi N. Generalized differential quadrature finite element method for cracked composite structures of arbitrary shape. Compos Struct 2013;106:815–34.

Please cite this article as: X.-W. Gao, L. F. Gao, Y. Zhang et al., Free element collocation method: A new method combining advantages of finite element and mesh free methods, Computers and Structures, https://doi.org/10.1016/j.compstruc.2019.02.002

[54] Fantuzzi N. New insights into the strong formulation finite element method for solving elastostatic and elastodynamic problems. Curved Layer Struct 2014;1:93–126.
[55] Tornabene F, Fantuzzi N, Ubertini F, Viola E. Strong formulation finite element method based on differential quadrature: a survey. Appl Mech Rev 2015;67 (2):1–55.
[56] Fantuzzi N, Tornabene F. Strong Formulation Isogeometric Analysis (SFIGA) for laminated composite arbitrarily shaped plates. Composites B 2016;96:173–203.
[57] Fantuzzi N, Tornabene F, Bacciocchi M, Neves AMA, Ferreira AJM. Stability and accuracy of three Fourier expansion-based strong form finite elements for the free vibration analysis of laminated composite plates. Int J Numer Meth Eng 2017;111:354–82.
[58] Fantuzzi N, Leonetti L, Trovalusci P, Tornabene F. Some novel numerical applications of cosserat continua. Int J Comput Methods 2018;15(3):1–38.
[59] Sladek V, Sladek J, Zhang C. Local integro-differential equations with domain elements for the numerical solution of partial differential equations with variable coefficients. J Eng Math 2005;51:261–82.
[60] Sladek V, Sladek J, Zhang CZ. Computation of stresses in non-homogeneous elastic solids by local integral equation method: a comparative study. Comput Mech 2008;41:827–45.
[61] Sladek V, Sladek J, Zhang C. The use of finite elements for approximation of field variables on local sub-domains in a mesh-free way. Netherlands: Springer; 2008. p. 87–106.
[62] Gao XW. Cross-line method (CLM) for solving partial differential equations. In: Proc of the 8th international conference on computational methods, Guilin City, July 25–29, 2017.
[63] Gao XW, Gao LF, Liu HY. A new numerical method – Free Element Collocation Method (FECM). In: Proc of the 13th world congress on computational mechanics/2nd Pan American congress on computational mechanics (WCCM 2018), New York City, NY, July 22–27, 2018.
[64] Gao XW, Davies TG. Boundary element programming in mechanics. Cambridge, UK: Cambridge University Press; 2002.
[65] Nguyen-Thanh N, Zhou K. Extended isogeometric analysis based on PHT-splines for crack propagation near inclusions. Int J Numer Meth Eng 2017;112:1777–800.
[66] Sun SH, Yu TT, Nguyen TT, Atroshchenko E, Bui TQ. Structural shape optimization by IGABEM and particle swarm optimization algorithm. Eng Anal Boundary Elem 2018;88:26–40.

Please cite this article as: X.-W. Gao, L. F. Gao, Y. Zhang et al., Free element collocation method: A new method combining advantages of finite element and mesh free methods, Computers and Structures, https://doi.org/10.1016/j.compstruc.2019.02.002